applied sciences

MDPI

Systematic Review

Applications of Deep Learning to Neurodevelopment in Pediatric Imaging: Achievements and Challenges

Mengjiao Hu [1], Cosimo Nardi [2], Haihong Zhang [1] and Kai-Keng Ang [1,3,*]

[1] Institute for Infocomm Research (I2R), Agency for Science, Technology and Research (A*STAR), Singapore 138632, Singapore
[2] Department of Experimental and Clinical Biomedical Sciences, University of Florence—Azienda Ospedaliero-Universitaria Careggi, 50134 Florence, Italy
[3] School of Computer Science and Engineering, Nanyang Technological University, Singapore 639798, Singapore
* Correspondence: kkang@i2r.a-star.edu.sg; Tel.: +65-64082678

Abstract: Deep learning has achieved remarkable progress, particularly in neuroimaging analysis. Deep learning applications have also been extended from adult to pediatric medical images, and thus, this paper aims to present a systematic review of this recent research. We first introduce the commonly used deep learning methods and architectures in neuroimaging, such as convolutional neural networks, auto-encoders, and generative adversarial networks. A non-exhaustive list of commonly used publicly available pediatric neuroimaging datasets and repositories are included, followed by a categorical review of recent works in pediatric MRI-based deep learning studies in the past five years. These works are categorized into recognizing neurodevelopmental disorders, identifying brain and tissue structures, estimating brain age/maturity, predicting neurodevelopment outcomes, and optimizing MRI brain imaging and analysis. Finally, we also discuss the recent achievements and challenges on these applications of deep learning to pediatric neuroimaging.

Keywords: pediatric; magnetic resonance imaging; neurodevelopment; deep learning

check for updates

Citation: Hu, M.; Nardi, C.; Zhang, H.; Ang, K.-K. Applications of Deep Learning to Neurodevelopment in Pediatric Imaging: Achievements and Challenges. *Appl. Sci.* **2023**, *13*, 2302. https://doi.org/10.3390/app13042302

Academic Editor: Qi-Huang Zheng

Received: 15 December 2022
Revised: 3 February 2023
Accepted: 8 February 2023
Published: 10 February 2023

Copyright: © 2023 by the authors. Licensee MDPI, Basel, Switzerland. This article is an open access article distributed under the terms and conditions of the Creative Commons Attribution (CC BY) license (https://creativecommons.org/licenses/by/4.0/).

1. Introduction

Machine learning has achieved extraordinary achievements during the past decades. Conventional machine learning algorithms such as support vector machine and logistic regression have been widely applied to image analysis for pattern recognition and identification [1]. Yet applications of such approaches are limited by the reliance on feature extraction procedure and restrictions on high dimensionality of data. Feature extraction requires high expertise in domain knowledge to transform raw data into a different representation. Further dimension reduction techniques are required to fit the high-dimensional features to the machine learning algorithms [2]. Evolution of deep learning algorithms such as convolutional neural networks has advanced the development of machine learning to another triumph. The end-to-end framework of deep learning allows automatic feature learning of the complicated data patterns which migrates the subjectivity in feature extraction procedure. The deep architecture and nonlinear processing units empower the deep learning algorithm to deal with a vast amount of data [3,4]. Successful applications of conventional machine learning and deep learning to medical imaging have been widely reported [5,6]. Specifically, neuroimaging studies based on magnetic resonance imaging (MRI) have applied machine learning to the study of the brain in many aspects [7,8].

MRI has become a crucial diagnostic imaging technique for the study of the brain for its advantage of non-ionic and high-contrast resolution [9]. MRI relies on the nuclear magnetic resonance phenomenon, in which atomic nuclei will re-emit radio signals when placed in a magnetic field and stimulated by oscillating radio waves. Human body contains rich hydrogen nuclei and the nuclei align to the magnetic field generated by the MRI

scanner. Then, an oscillating radio frequency deviates the magnetic momentum of the nuclei from the field. When the oscillating radio pulse is removed, signals generated by the realignment of hydrogen nuclei can be detected by a reciever coil [10,11]. The most common MRI modality is the structural MRI (sMRI) which provides morphostructural information based on the concentration of hydrogen protons. sMRI measures the signals produced by aligned hydrogen protons in water molecules in the body and creates excellent contrast among different tissues. Functional MRI (fMRI) quantifies the blood oxygenation level-dependent (BOLD) signals based on the blood flow and blood oxygen changes around cells and reflects the brain activity information [12]. Resting-state fMRI (rs-fMRI) is measured when the subject is at rest while task fMRI monitors the brain function during an assigned task. Diffusion tensor imaging (DTI) estimates the motion of water molecules in the brain. The water molecules' diffusion speed and directions are restricted by tissue types and fiber architectures. DTI therefore provides information based on the quantitative anisotropy and orientation [13]. Deep learning methods have been widely applied to neuroimaging studies in adult for neuropsychiatric disorder recognition, brain tissues and structures segmentation, and clinical outcome prediction [8,14,15]. In comparison, relatively few deep learning studies have been conducted in pediatric MRI. Most previous reviews on pediatric MRI involved a large number of studies using conventional machine learning approaches instead of deep learning algorithms and some reviews focused on specific topics such as Autism [7,16,17]. To illustrate the most recent achievements of deep learning in pediatric MRI, this systematic review summarized the advanced deep learning approaches applied to multiple neurodevelopmental topics in MRI-based research in the past five years. Section 2 introduces the most commonly utilized deep learning algorithms as well as a list of available public datasets for neurodevelopment. Section 3 categorizes the recent studies into five main topics: recognizing neurodevelopmental disorders, identifying brain and tissue structures, estimating brain age/maturity, predicting neurodevelopment outcomes, and optimizing MRI brain imaging and analysis. The challenges and insights of applying deep learning to pediatric MRI are discussed in Section 4. We conclude in Section 5.

2. Methods

2.1. Deep Learning Model Architectures

Multi-layer perceptron (MLP) has the most basic architecture of deep neural networks, which is composed a stack of processing layers: an input layer, several hidden layers, and an output layer (Figure 1) [18]. The neurons in the processing layers allow nonlinear computation and empower the model to learn different representations of the training data at multiple levels of abstraction [3].

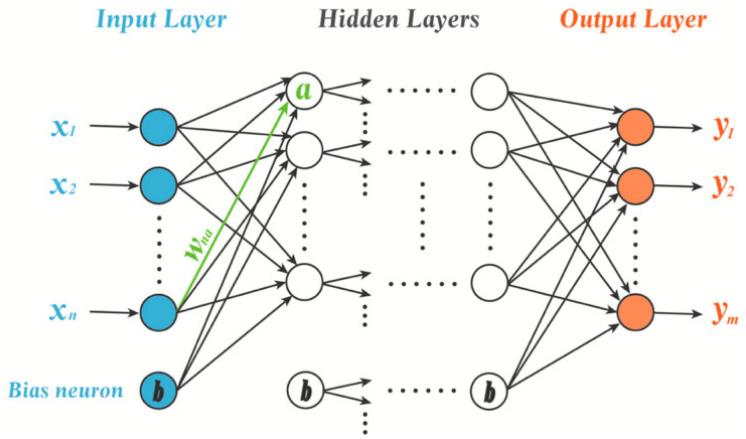

Figure 1. Architecture of multi-layer perceptron (MLP) [18].

Convolutional neural network (CNN) is the most widely applied deep learning algorithm for medical imaging studies. A typical CNN consists of convolutional layers with

activation functions, pooling layers, and fully connected layers (Figure 2) [2]. Convolutional layers convolve an image with different types of kernel functions to extract image features. The kernels are applied to the entire image, thus greatly reducing the number of weights to be trained compared to fully connected neural networks. Activation functions such as sigmoid and ReLu (Rectified Linear Unit) serve as nonlinear feature detectors to introduce nonlinearities to CNN. Pooling layers reduce feature map resolution with translational invariance. The combination of convolutional and pooling layers enables CNN to learn spatial hierarchies among feature patterns. Fully connected layers function as a classifier or regressor to predict the desired outcomes [2]. The weight sharing and translational invariance properties facilitate CNN the efficient and precise power on image processing tasks. Depending on the input data dimensionality, 1D, 2D, and 3D convolutional kernels can be employed. Besides the basic stacking of convolutional layers, pooling layers and fully connected layers, models with complex architectures have been developed to further improve the performance of CNN. AlexNet was the first big CNN model which showed the great potential of CNN on image recognition tasks [19]. Inception blocks utilize convolution kernels of different sizes at the same level to optimize the accuracy and computation time of the model [20]. Residual connection from a previous layer to a later layer without extra parameters solves the vanishing gradients issues and thereby make the CNN model with many layers [21]. Dense blocks formed by many convolution operations and a final pooling and connecting the input and output of each convolution are proposed to train even deeper models [22]. Many other CNN models with different architectures have been proposed. A detailed summary can be found in the review paper by Celard et al. [2].

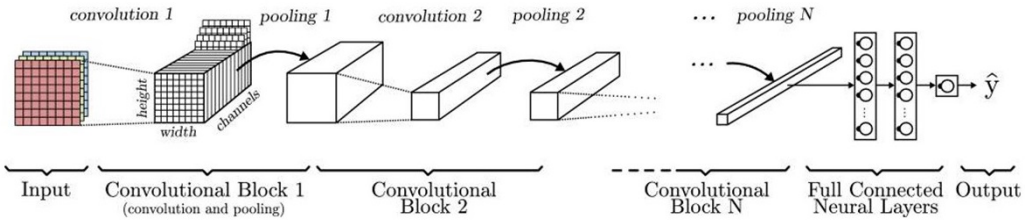

Figure 2. Architecture of convolutional neural networks [2].

U-net was proposed for semantic segmentation in 2015 and is still one of the most used CNN architectures for medical image segmentation. The typical U-net is composed of symmetrical encoder and decoder paths connected by skip connections (Figure 3) [23]. The model first performs a set of convolutions at the encoder side to extract features from the input data and then reconstructs the input image while including new information by transposed convolutions at the decoder side. Skip connections connect the encoder and decoder at each level. Complex architectures have also been applied to U-net to further improve its performance, for example, the Res-U-net and U-net with attention mechanism [24,25].

Auto-encoder plays a pivotal role in unsupervised deep learning. Auto-encoder follows the encoder and decoder architecture (Figure 4). The encoder aims at learning a latent representation with low dimensionality which retains only the significant information while ignoring the noise. The decoder utilizes the latent representation to reconstruct the input data. Auto-encoder provides an effective approach for feature learning in recognition tasks with unlabeled data. Variational auto-encoders are applied as generative models which randomly generate new data that are similar to the input data [2].

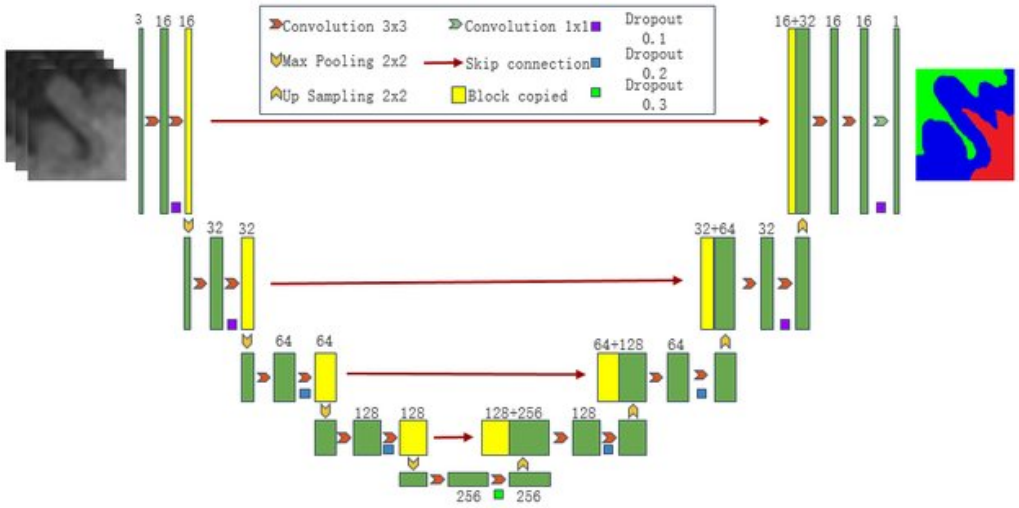

Figure 3. Architecture of U-net [26].

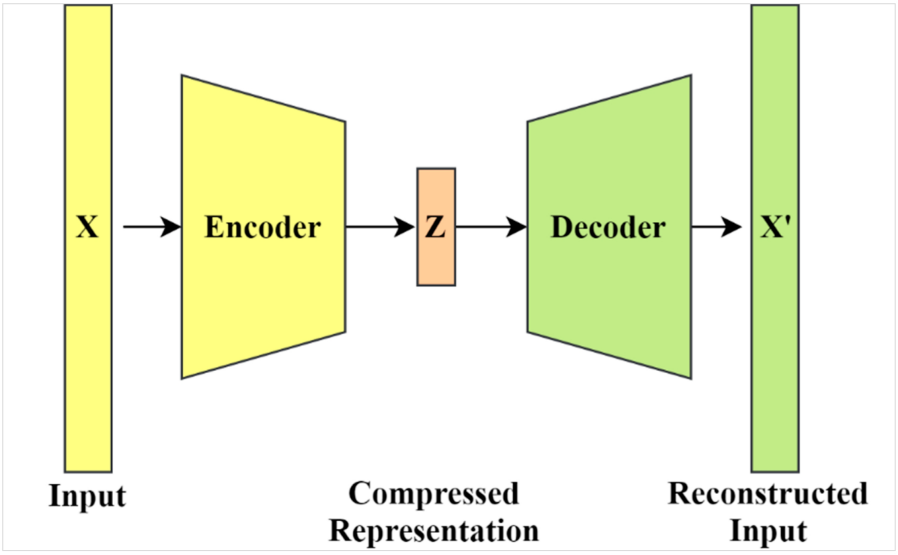

Figure 4. Architecture of auto-encoder [27].

Generative adversarial network (GAN) has attracted attention with its ability to model data distributions and generate realistic data since proposed in 2014 [28]. GAN consists of one generator network which captures the data distribution in real images and generates a fake image and one discriminator which classifies the generated fake images and real images (Figure 5). Two networks are trained alternatively in a competitive manner. A large number of variations of GAN have been proposed and applied to object detection, localization, segmentation, data augmentation, and image quality improvement tasks [29]. A review paper [30] introduced various architectures of GAN and their applications in medical imaging.

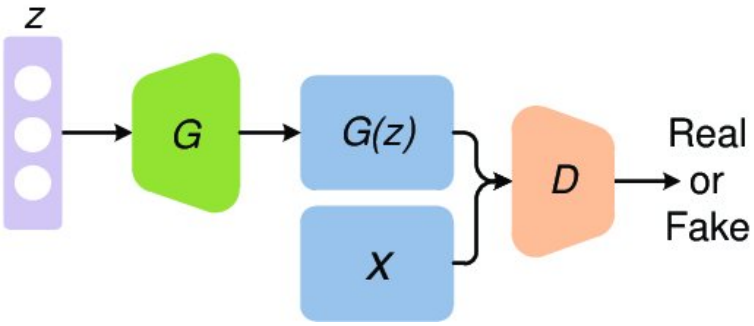

Figure 5. Architecture of generative adversarial networks (GAN) [29].

2.2. Public Datasets and Repositories

Sample size is one of the most critical issues for training a deep learning algorithm as the number of trainable parameters grows exponentially with deep architectures. However, data collection is expensive and time-consuming for medical images. Fortunately, more and more data repositories and data-sharing platforms are available recently, making it possible to conduct medical imaging studies on a large scale. Table 1 lists the available public datasets and repositories involved in the studies reviewed in this manuscript. Some repositories collect data from multiple independent sites and provide a large number of subjects. The Autism Brain Imaging Data Exchange (ABIDE) dataset and IMaging-PsychiAtry Challenge (IMPAC) dataset focus on autism spectrum disorder (ASD) recognition and provide data of subjects with ASD and healthy controls. The ADHD-200 consortium collects data for attention deficit hyperactivity disorder (ADHD) patients and healthy controls. The Healthy Brain Network (HBN) dataset and Human Connectome Project Development (dHCP) project are data collections for typically developed individuals. The UNC/UMN Baby Connectome Project (BCP) collects data of infants and pre-school age children. Other datasets including a large number of participants such as UK Biobank and International Consortium for Brain Mapping (ICBM) involve healthy controls as well as patients with various neurodevelopmental disorders at all ages.

Table 1. Public datasets.

Dataset	No. of Sites/Projects	Population	Technique	Citation
Autism Brain Imaging Data Exchange I (ABIDE I)	17 independent imaging sites	539 subjects with ASD and 573 healthy controls (age 7–64 years)	sMRI, rs-fMRI	[31]
Autism Brain Imaging Data Exchange II (ABIDE II)	19 independent imaging sites	521 subjects with ASD and 593 healthy controls (age 5–64 years)	sMRI, rs-fMRI, DTI	[32]
IMaging-PsychiAtry Challenge (IMPAC)	-	549 subjects with ASD 601 healthy controls (age 0–80 years)	sMRI, rs-fMRI	[33]
ADHD-200 Consortium	8 independent imaging sites	285 subjects with ADHD 491 healthy controls (age 7–21 years)	sMRI, rs-fMRI	[34]
UK Biobank	-	500,000 subjects (age 40–69 years)	sMRI, rs-fMRI, DTI	[35]

Table 1. *Cont.*

Dataset	No. of Sites/Projects	Population	Technique	Citation
National Database for Autism Research (NDAR)	hundreds of research projects	117,573 subjects by age (57,510 affected subjects and 59,763 control subjects)	sMRI, rs-fMRI, DTI	[36]
Open fMRI	95 datasets	3375 subjects across all datasets	sMRI, rs-fMRI, task fMRI	[37]
International Consortium for Brain Mapping (ICBM)	-	853 subjects (age 18–89 years)	sMRI, rs-fMRI, DTI	[38]
1000 funtional connectome	33 independent imaging sites	1355 subjects (age 13–80 years)	rs-fMRI	[39]
The Adolescent Brain Cognitive Development (ABCD) Study	-	12,000 subjects (age 9–10 years)	sMRI, rs-fMRI, task fMRI	[40]
ENIGMA ADHD working group	34 cohorts	over 4000 subjects	sMRI, rs-fMRI, DTI	[41]
Philadelphia Neurodevelopmental Cohort (PNC)	-	9500 subjects (age 8–21 years)	sMRI, rs-fMRI, task fMRI, DTI	[42]
Healthy Brain Network (HBN)	-	10,000 subjects (age 5–21 years)	sMRI, rs-fMRI, task fMRI, DTI	[43]
Human Connectome Project Development (dHCP)	-	1350 subjects (age 5–21 years)	sMRI, rs-fMRI, task fMRI	[44]
The UNC/UMN Baby Connectome Project (BCP)	2 sites	500 subjects (age 0–5 years)	sMRI, rs-fMRI, DTI	[45]

Abbreviations: sMRI—structural MRI, rs-fMRI—resting-state functional MRI, DTI—Diffusion Tensor Imaging.

2.3. Review Parameters

The paper selection and review procedure in this study follows the preferred reporting items for systematic reviews and meta-analysis (PRISMA) guidelines [46,47]. The search terms employed were <deep learning brain MRI neurodevelopment> or <deep learning pediatric brain MRI> or <deep learning child brain MRI> or <deep learning adolescent brain MRI> to include the deep learning studies based on MRI for pediatric neurodevelopment studies. The initial search was performed on PubMed and Web of Science databases on 26 October 2022. Search engines ScienceDirect and Google Scholar were excluded due to the large number of search results returned (thousands of results).

The initial search yielded 412 papers from PubMed and 252 papers from Web of science. Following the PRISMA protocols, we performed selection and review steps in Figure 6. A total of 304 duplicate records was removed in the first step. Secondly, we examined the keywords, titles, and abstracts of the remaining 360 papers and excluded review papers, case reports, papers with foreign language (French), and animal studies. Furthermore, we identified studies with topics on adult population, genetics, maternity, and non-deep learning approaches as irrelevant and excluded them. We retrieved the full paper for 184 out of the remaining 185 studies. The full papers were further examined for eligibility and 67 studies with non-pediatric population, non-MRI modality or non-deep learning methods were removed. Then, 120 Studies were carefully reviewed and 113 of them are categorized and reported in the next chapter. The remaining 7 studies on gender prediction, functional connectivity estimation, and fascicles detection are not reported.

Three researchers independently examined the eligibility of the studies and conflict decisions were resolved by discussion. Data extracted from selected studies include but are not limited to the year of the study, clinical questions, study population, imaging techniques, preprocessing protocols and tools, deep learning approach, training and validation settings,

results, results interpretation, and limitations. Extracted information is presented and discussed in the following chapters. Specifically, risk of bias analysis was performed following the Risk Of Bias In Non-randomized Studies of Interventions [48] for (1) risk of bias due to confounding; (2) risk of bias in selection of participants into the study; (3) risk of bias in classification of interventions; (4) risk of bias due to deviations from intended interventions; (5) risk of bias due to missing data; (6) risk of bias arising from measurement of outcomes; (7) risk of bias in selection of reported results. Risk of bias analysis is presented in Appendix A (Table A1).

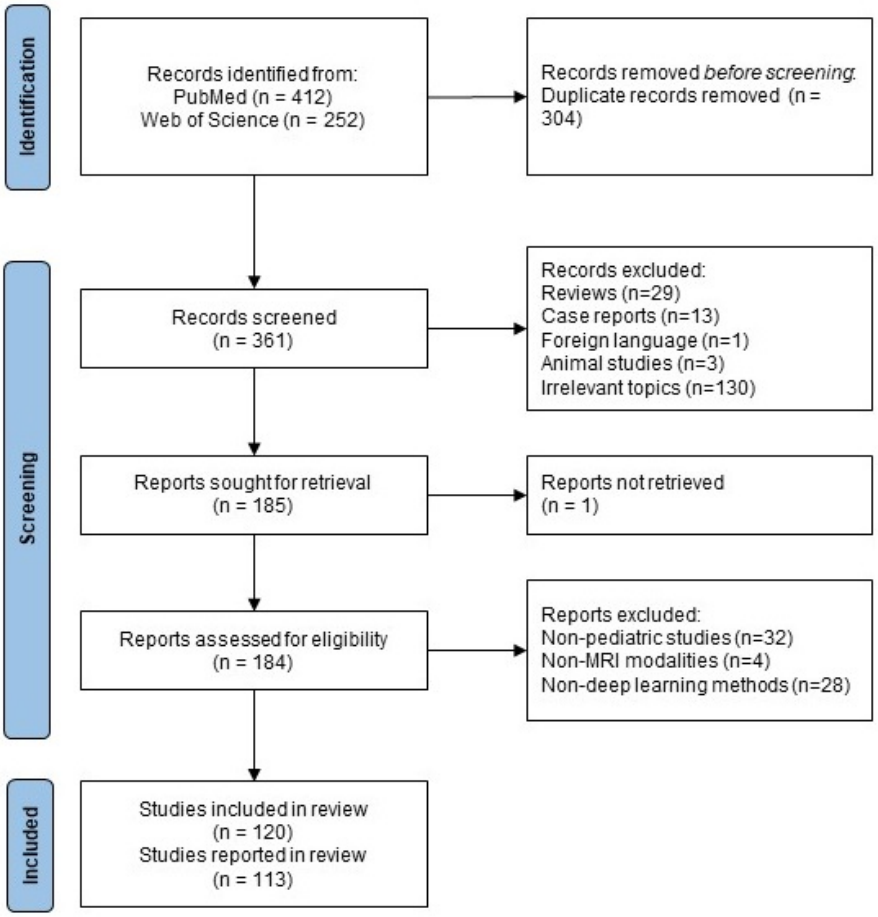

Figure 6. Study selection procedure.

3. Results

3.1. Recognizing Neurodevelopmental Disorders

Neurodevelopmental disorders are common brain disorders in children, bringing a variety of challenges to the affected patients and causing great burdens to their families. Various genetic and environmental factors may perturb the developmental process and result in neurodevelopmental disorders [49].

Autism spectrum disorder (ASD) is one of the most common neurodevelopmental disorders [50]. ASD is characterized by early deficits in social interactions and communication accompanied by restricted and repetitive behaviors [49]. Review papers [7,17] summarized a selected number of studies using artificial intelligence approaches to classify ASD patients and healthy controls including both conventional machine learning methods and deep learning methods. This review listed the recent deep learning advancements using MLP, CNN, RNN, and auto-encoder models (Table 2). Rs-fMRI is widely utilized for ASD recognition. Connectomes derived from fMRI were used as inputs to MLP, CNN,

and RNN for classification [51–54]. A multimodal study [55] combined sMRI, rs-fMRI, and task fMRI.

Attention deficit hyperactivity disorder (ADHD) is another common neurodevelopmental disorder [50]. ADHD patients often suffer from hyperactivity, impulsivity, and inattention, and ADHD often continues to adulthood [56]. Previous ADHD recognition studies were summarized in the review paper [7] in conventional machine learning category and deep learning category. This review paper focuses on more recent studies utilizing deep learning approaches for ADHD detection (Table 2). Both rs-fMRI and sMRI are employed as inputs for deep learning networks.

Neurodevelopmental disorders which are less common such as cerebellar dysplasia [57], dyslexic [58], epilepsy [59,60], conduct disorder [61], disruptive behavior disorder [62], and post-traumatic stress disorder [63] are also reviewed in this study. We also include three studies for detection of posterior fossa tumors and tubers in tuberous sclerosis complex [64–66], and two studies for white matter pathway classification [67,68]. This review aims to investigate the deep learning methods utilized in various pediatric topics in an overall manner and therefore includes multiple disorders. Structural imaging techniques such as sMRI and DTI are more commonly utilized in these studies.

Overall, the selected studies are summarized in Table 2. Most studies conducted baseline comparisons using conventional machine learning approaches and reported the superior performance of deep learning approaches [53,69]. CNN dominates in the image recognition tasks. A total of 41 out of 48 neurodevelopmental disorder classification studies in this review utilized CNN approaches. Advanced CNN architectures such as inception and residual modules were employed in 2D CNN models [70–72]. Several studies trained 3D CNN with a limited number of sample size [61,69,73,74], bringing concerns on overfitting. Large-scale studies which involve thousands of training data were conducted using public datasets and repositories [55,75–78]. Multimodal studies combined features from multiple MRI modalities showed better performance than single modality [62,76].

Table 2. Recognizing neurodevelopmental disorders.

Study	Year	Disorder	Population	Technique	Preprocessing	Method	Results
[79]	2017	Autism	ABIDE I dataset 55 ASD (age 14.2 ± 3.2 years) 55 HC (age 12.7 ± 2.4 years)	rs-fMRI	Preprocessed Connectomes Project	MLP	Accuracy 86.36%
[80]	2018	Autism	62 ASD 48 HC	task fMRI	FSL	MLP	Accuracy 87.1%
[51]	2018	Autism	ABIDE I dataset 529 ASD 571 HC	rs-fMRI	In-house pipeline	RNN	Accuracy 70.1%
[81]	2018	Autism	ABIDE I & II dataset 116 ASD 69 HC (age 5–10 years)	sMRI, rs-fMRI	SPM8	Deep Belief Network	Accuracy 65.56%
[53]	2019	Autism	ABIDE I & II dataset 210 ASD 249 HC (age 5–10 years)	rs-fMRI	SPM8	CNN	Accuracy 72.73%
[52]	2019	Autism	ABIDE II dataset 117 ASD 81 HC (age 5–12 years)	rs-fMRI	FSL	Auto-encoder	Accuracy 96.26%

Table 2. *Cont.*

Study	Year	Disorder	Population	Technique	Preprocessing	Method	Results
[55]	2020	Autism	multi datasets: ABCD, ABIDE I, II, BioBank, NDAR, ICBM, Open fMRI, 1000 Functional Connectomes 43,838 total connectomes 1711 ASD (age 0.42–78 years)	rs-fMRI, task-fMRI	SPT, AFNI, SpeddyPP	CNN	AUROC 0.6774
[82]	2020	Autism	YUM dataset 40 ASD (age 29.4 ± 11.6 years) 33 HC (age 30.1 ± 5.3 years) ABIDE I dataset 521 ASD (age 29.4 ± 11.6 years) 593 HC (age 30.1 ± 5.3 years)	sMRI	SPM8	3D CNN	Accuracy 88% (YUM) 64% (ABIDE)
[69]	2021	Autism	ABIDE I dataset 55 ASD (age 14.52 ± 6.97 years) 55 HC (age 15.81 ± 6.25 years)	rs-fMRI	Configurable Pipeline for the Analysis of Connectomes	3D CNN	Accuracy 77.74%
[74]	2021	Autism	50 ASD 50 HC (age 12–40 months)	task-fMRI	FSL, FEAT	3D CNN	Accuracy 80%
[83]	2021	Autism	ABIDE I & II dataset 1060 ASD 1146 HC (age 5–64 years)	rs-fMRI	In-house pipeline	CNN	Accuracy 89.5%
[84]	2021	Autism	ABIDE I dataset 506 ASD 532 HC (age 10–28 years)	rs-fMRI	DPABI	MLP	Accuracy 78.07 ± 4.38%
[85]	2021	Autism	52 ASD 195 HC infants (age 24 months)	MRI	iBEAT	CNN	Accuracy 92%
[76]	2021	Autism	multi datasets: ABCD, ABIDE I, II, BioBank, NDAR, Open fMRI 29,288 total connectomes 1555 ASD (age 0.42–78 years)	sMRI, rs-fMRI, task-fMRI	AFNI, SpeddyPP	CNN	AUROC 0.7354
[54]	2022	Autism	ABIDE & UM dataset 411 HC for offline learning 48 ASD 65 HC for testing (age 13.8 ± 2 years)	rs-fMRI	Connectome Computation System	Auto-encoder	Accuracy 67.2%
[73]	2022	Autism	Preschool dataset 110 subjects ABIDE I dataset 1099 subjects	sMRI	SPM8	CNN	AUROC 0.787 (preschool) 0.856 (ABIDE)
[86]	2022	Autism	151 ASD 151 HC (age 1–6 years)	sMRI	In-house pipeline	3D CNN	Accuracy 84.4%
[75]	2022	Autism	IMPAC dataset 418 ASD 497 hc (age 17 ± 9.6 years)	sMRI, rs-fMRI	In-house pipeline	MLP	AUROC 0.79 ± 0.01

Table 2. *Cont.*

Study	Year	Disorder	Population	Technique	Preprocessing	Method	Results
[87]	2019	ADHD	ADHD-200 consortium 776 subjects	rs-fMRI	In-house pipeline	3D CNN	Accuracy 69.01%
[88]	2020	ADHD	ADHD-200 consortium 262 subjects	rs-fMRI	AFNI, FSL	CNN	Accuracy 73.1%
[78]	2021	ADHD	ENIGMA-ADHD Working Group 2192 ADHD 1850 HC (age 4–63 years)	sMRI	FreeSurfer	MLP	Testing AUROC 0.60
[89]	2022	ADHD	ADHD-200 consortium NI site25 ADHD 23 HC (age 11–22 years) NYU site: 118 ADHD 98 HC (age 7–18 years) KKI site: 22 ADHD 61 HC (age 8–13 years) PU site: 78 ADHD 116 HC (age 8–17 years) PU-1 site: 24 ADHD 62 HC (age 8–17 years)	rs-fMRI	Preprocessed Connectomes Project	Auto-encoder	Accuracy >99%
[90]	2022	ADHD	ADHD-200 consortium NI site: 28 ADHD-I 37 HC NYU site: 72 ADHD-I, 42 ADHD-C, 96 HC OHSU site: 27 ADHD-I, 13 ADHD-C, 70 HC KKI site: 16 ADHD-I, 5 ADHD-C 60 HC PU-1 site: 16 ADHD-I, 26 ADHD-C, 88 HC PU-2 site: 15 ADHD-I, 20 ADHD-C, 31 HC PU-3 site: 7 ADHD-I, 12 ADHD-C, 23 HC	rs-fMRI	DPABI	CNN	Accuracy >99%
[91]	2022	ADHD	ADHD-200 consortium Training: 69 ADHD 99HC Testing: 24 ADHD 27 HC (age 7–21 years	rs-fMRI	Athena pipeline	CNN	Testing accuracy 67%
[77]	2022	ADHD	ADHD-200 consortium 325 ADHD 547 HC (age 12 ± 3.0 years)	rs-fMRI	Athena pipeline	CNN	Accuracy 78.7 ± 4.3%
[92]	2022	ADHD	19 ADHD (age 10.25 ± 1.94 years) 20 HC (age 10.15 ± 2.13 years)	sMRI	SPM	CNN	Accuracy 93.45 ± 1.18%
[93]	2022	ADHD	ABCD Dataset 127 ADHD 127 HC (age 9–10 years)	sMRI	ANTs	CNN	Accuracy 71.1%
[57]	2018	Cerebellar Dysplasia	90 patients, 40 HC	sMRI	FSL, ANTs	3D CNN	Accuracy 98.5 ± 2.41%
[61]	2020	Conduct Disorder	60 patients (age 15.3 ± 1.0 years) 60 HC (age 15.5 ± 0.7 years)	sMRI	-	3D CNN	Accuracy 85%

Table 2. *Cont.*

Study	Year	Disorder	Population	Technique	Preprocessing	Method	Results
[62]	2021	Disruptive Behavior Disorder	ABCD Study: 550 patients, 550 HC (age 9–11 years)	sMRI, rs-fMRI, DTI	FSL	3D CNN	Accuracy 72%
[58]	2020	Dyslexic	36 patients, 19 HC (age 9–12 years)	task fMRI	SPM	3D CNN	Accuracy 72.73%
[94]	2020	Embryonic Neurodevel-opmental Disorders	114 patients, 113 HC (age 16–39 weeks)	sMRI	—	CNN	Accuracy 87.7%
[59]	2020	Epilepsy	30 patients, 13 HC	sMRI	BET	CNN	Accuracy 66–73%
[60]	2020	Epilepsy	59 patients, 70 HC (age 7–18 years)	DTI	SPM	CNN	Accuracy 90.75%
[70]	2021	Neonatal Hyperbiliru-binemia	47patients, 32 HC (age 1–18 days)	sMRI		CNN	Accuracy 72.15%
[63]	2021	PTSD	33 patients (age 14.3 ± 3.3 years) 53 HC (age 15.0 ± 2.3 years)	rs-fMRI	SPM12	MLP	Accuracy 72%
[64]	2020	Tuber	260 patients, 260 HC	sMRI	FSL	3D CNN	Accuracy 97.1%
[65]	2022	Tuber	296 patients, 245 HC (age 0–8 years)	sMRI	-	3D CNN	Accuracy 86%
[71]	2020	Tuber	114 patients (age 5–15.3 years), 114 HC (age 6.9–15.7 years)	sMRI	In-house pipeline	CNN	Accuracy 95%
[95]	2021	Tumor	136 patients, 22 HC (age 0–11 years)	sMRI	SPM	CNN	Accuracy 87 ± 2%
[72]	2020	Tumor	617 patients with tumor (age 0.2–34 years)	sMRI	Pydicom	CNN	Accuracy 72%
[66]	2018	Tumor	233 subjects	sMRI	-	Capsule Network	Accuracy 86.56%
[96]	2020	Tumor	39 pediatric patients	sMRI	-	CNN	Accuracy 87.8%
[67]	2020	White Matter Pathways	89 patients with focal epilepsy (age 9.95 ± 5.41 years)	DTI	FreeSurfer	CNN	Accuracy 98%
[68]	2019	White Matter Pathways	70 HC (age 12.01 ± 4.80 years), 70 patients with focal epilepsy (age 11.60 ± 4.80 years)	DTI	FreeSurfer, FSL, NIH TORTOISE	CNN	F1 score 0.9525 ± 0.0053

Abbreviations: ASD—Autism spectrum disorder, HC—healthy control, ADHD—Attention deficit hyperactivity disorder, sMRI—structural MRI, rs-fMRI—resting-state functional MRI, DTI—Diffusion Tensor Imaging, MLP—Multi-layer perceptron, CNN—Convolutional neural network.

3.2. Identifying Brain and Tissue Structures

Identifying brain and tissue structures is of great importance in facilitating studies investigating changes in a specific region of interest. Accurate segmentation of brain tissues and structures lays the foundation for volumetric and morphologic analysis. Volumetric

analysis of gray matter, white matter, cerebrospinal fluid, and specific brain structure such as amygdala assist in computer-aided diagnosis of neurodevelopmental disorders. Localization and segmentation of brain tumor is essential for assessment of the tumor burden as well as treatment response and tumor progression [97]. Brain masking isolates the brain from surrounding tissues across non-stationary 3D brain volumes in fMRI, which is important and challenging, especially for fetal imaging [98]. Specific challenges for pediatric brain segmentation exist due to the variations in head size and shape in children compared to adults. Rapid changes in tissue contrast and low contrast to noise ratio in fetal and newborn MRIs lead to further demanding techniques [99]. This study reviews segmentation of pediatric brain tissues, structures, tumors, and masking of fetal brain (Table 3).

Most of the studies employed U-net for segmentation. Dice scores vary across studies. 3D U-net models were implemented for brain tissue and volume segmentation [25,100–102]. Transfer learning and active learning greatly reduced the number of samples that need to be labeled for training a high-quality patch-wise segmentation method [99]. FetalGAN was proposed to segment a fetal functional brain MRI using a segmentor as the generator in GAN architecture and achieved better performance than 3D U-net [98]. Adversarial domain adaptation was used to adapt a pre-trained U-net to another segmentation task in an unsupervised learning manner [103]. Transfer learning and GAN stand for the opportunity of training segmentation algorithms with weakly labeled or unlabeled data, which may greatly reduce the tedious and time-consuming process of creating groundtruth for segmentation tasks.

Table 3. Identifying brain and tissue structures.

Study	Year	Structure	Population	Technique	Preprocessing Method	Results
[104]	2020	Amygdala	171 infants (age 6 months) 204 infants (age 12 months) 201 infants (age 24 months)	sMRI	- U-net	Dice score 0.882 (6-month) 0.882 (12-month) 0.903 (24-month)
[105]	2020	Anterior Visual Pathway	18 subjects	sMRI	- GAN	Dice score 0.602 ± 0.201
[106]	2018	Brain Mask	10 adolescent subjects (age 10–15 years), 25 newborn subjects from dHCP dataset	sMRI	- CNN	F1 score 95.21 ± 0.94 (adolescent) 90.24 ± 1.84 (newborns)
[99]	2019	Brain Mask	10 adolescent subjects, 26 newborn subjects from dHCP dataset, 25 other subjects (age 0.2–2.5 years)	sMRI	- CNN	Improve dice score after labeling a very small portion of target dataset (<0.25%)

Table 3. *Cont.*

Study	Year	Structure	Population	Technique	Preprocessing	Method	Results
[107]	2020	Brain Mask	197 fetuses (gestation age 24–39 weeks)	rs-fMRI	FSL	U-net	Dice score 0.94
[98]	2020	Brain Mask	71 scans of fetuses	rs-fMRI	AFNI	GAN	Dice score 0.973 ± 0.013
[108]	2020	Brain Mask	37 healthy fetuses (gestation age 27.3 ± 4.11 weeks) 32 fetuses with spina bifida pre-surgery (gestation age 23.06 ± 1.64 weeks) 16 fetuses post-surgery (gestation age 25.69 ± 1.21 weeks)	sMRI	-N4ITK	U-net	Dice score 0.9321 (healthy), 0.9387 (pre-surgery), 0.9294 (post-surgery)
[101]	2021	Brain Mask	214 fetuses (gestation age 22–38 weeks)	sMRI	-	3D U-net	Testing dice score 0.944
[109]	2021	Brain Mask	30 subjects (ages 2.34–4.31 years)	sMRI	-	CNN	Dice score 0.90 ± 0.14
[110]	2019	Brain Tissue	29 subjects (age 9.96 ± 7.16 years)	sMRI	-	3D CNN	Dice score 0.888 (gray matter), 0.863 (white matter), 0.937 (CSF)
[111]	2019	Brain Tissue	12 fetuses (gestation age 22.9–34.6 weeks)	sMRI	-	CNN	Dice score 0.88
[112]	2019	Brain Tissue	95 very pre-term infants (gestation age 28.5 ± 2.5 weeks, scan at term age), 28 very pre-term infants (gestation age 26.8 ± 2.1 weeks, scan at term age)	sMRI	-	CNN	Dice score 0.895 ± 0.098 testing dice score 0.845 ± 0.079
[113]	2020	Brain Tissue	47 patients with pediatric hydrocephalus (age 5.8 ± 5.4 years)	sMRI	-	CNN	Dice score 0.86
[114]	2021	Brain Tissue	35 subjects (age 4.2 ± 0.7 years)	sMRI	-	3D CNN	JS = 0.83 for gray matter JS = 0.92 for white matter
[25]	2021	Brain Tissue	98 preterm infants (gestation age $\leq$ 32 weeks)	DTI	In-house pipeline	3D U-net	Dice score 0.907 ± 0.041
[102]	2022	Brain Tissue	106 fetuses (gestation age 23–39 weeks)	sMRI	FSL	3D U-net	Dice score 0.897
[115]	2022	Brain Tissue	dHCP datast: 150 term (gestation age 37–44 weeks) 50 preterm (gestation age $\leq$ 32 weeks, scan at term-equivalent age)	sMRI	-	CNN	Dice score 0.88
[116]	2022	Brain Tissue	23 infants (age 6 ± 0.5 months)	sMRI	In-house pipeline	U-net	Dice score 0.92 (gray matter), 0.901 (white matter), 0.955 (CSF)

Table 3. *Cont.*

Study	Year	Structure	Population	Technique	Preprocessing	Method	Results
[117]	2020	Cerebral Arteries	48 subjects (age 0.8–22 years)	sMRI	In-house pipeline	U-net	Testing dice score 0.75
[118]	2021	Cerebral Ventricle	200 patients with obstructive hydrocephalus (age 0–22 years) 199 HC (age 0–19 years)	sMRI	In-house pipeline	U-net	Dice score 0.901
[103]	2021	Cortical Parcellation Network	dHCP datast: 403 infants, ePRIME dataset: 486 infants (gestation age 23–42 weeks, scanned at term-equivalent age)	sMRI	-MRITK	GAN	Dice score 0.96–0.99
[119]	2020	Cortical Plate	52 fetuses (gestation age 22.9–31.4 weeks)	sMRI	In-house pipeline	CNN	Testing dice score 0.907 ± 0.027
[120]	2021	Cortical Plate	12 fetuses (gestation age 16–39 weeks)	sMRI	-AutoNet, ITK-SNAP	CNN	Dice score 0.87
[121]	2019	Intracranial Volume	80 scans of fetuses (gestation age 22.9–34.6 weeks) 101 scans of infants (age 30–44 weeks)	sMRI	-	U-net	Dice score 0.976
[122]	2022	Limbic Structure	dHCPdataset: 473 subjects (40.65 ± 2.19)	sMRI	-	CNN	Dice score 0.87
[123]	2022	Posterior Limb of Internal Capsule	450 preterm infants (gestation age $\leq$ 32 weeks, scan at term-equivalent age)	sMRI	In-house pipeline	U-net	Dice score 0.690
[124]	2022	Tuber	29 subjects (age 9.96 ± 7.16 years)	sMRI	-	U-net	Testing dice score 0.59 ± 0.23
[125]	2022	Tumor	311 pediatric subjects	sMRI	-	U-net	Dice score 0.773
[126]	2022	Tumor	177 patients (age 0.27–17.87 years)	sMRI	CaPTk software	CNN	Dice score 0.910
[100]	2022	Tumor	122 patients (age 0.2–17.9 years)	sMRI	ANTs	3D U-net	Dice score 0.724
[97]	2022	Tumor	BraTS 2020 Dataset: 369 patients local dataset: 22 patients (average age 7.5–9 years)	sMRI	In-house pipeline	U-net	Dice score 0.896

Abbreviations: sMRI—structural MRI, rs-fMRI—resting-state functional MRI, DTI—Diffusion Tensor Imaging, CNN—Convolutional neural network, GAN—Generative adversarial network.

3.3. Predicting Brain Age

The brain development of children experiences a rapid and complex stage, especially for children younger than two years. Early brain development is critical for cognitive, sensory, and motor ability. Delayed brain development can lead to many neurodevelopmental disorders in children and affect their quality of life [127]. Accurate evaluation of brain development via brain age estimation based on neuroimaging is of clinical importance to understand healthy brain development and study the brain maturity deviation caused by neurodevelopmental disorders [128].

We summarized age prediction studies involved both infants and young children (Table 4). Structural MRI techniques are commonly utilized in 2D and 3D CNN models.

Study [128] using 2D CNN on DTI achieved comparison results with human experts. Study [127] demonstrated superior performance of 3D CNN compared to conventional machine learning approaches and 2D CNN. Multimodal study [129] combined sMRI, rs-fMRI, and DTI features and yielded a mean absolute error of 0.381 years for children and adolescents aged 8–21 years old. The age difference for the study population varies and thus reporting of the relative error rate is necessary for comparing different methods in different studies.

Table 4. Predicting brain age.

Study	Year	Population	Technique	Preprocessing	Method	Results
[84]	2017	115 infants (gestation age 24–32 weeks)	DTI	In-house pipeline	CNN	MAE 2.17 weeks
[130]	2019	317 MRI images of 112 infants age 2 weeks (8 to 35 days); 12 months (each ±2-weeks) and 3 years (each ±4-weeks).	sMRI	In-house pipeline	3D CNN	Accuracy 98.4% classifying three age groups
[131]	2019	PNC Dataset: 857 subject (age 8–22 years) 20% as children 20% as young adult	rs-fMRII	SPM12	MLP	Accuracy 96.64% predicting children and young adult
[132]	2020	ABIDE II dataset 382 subjects ADHD200 consortium 378 subjects	sMRI	SPM12	3D CNN	MAE 1.11 years (ABIDE II dataset) 1.16 years (ADHD200 consortium)
[127]	2020	220 subjects (age 0–5 years)	sMRI	In-house pipeline	CNN	MAE 2.26 months
[129]	2020	PNC Dataset: 839 subject (age 8–21 years)	sMRI, rs-fMRI, DTI	SPM12, DPARSF, PANDA	MLP	MAE 0.381 ± 0.119 years
[128]	2021	161 subjects (age 0–2 years)	sMRI	In-house pipeline	CNN	MAE 8.2 weeks
[133]	2021	84 infants (age 8 days–3 years)	sMRI	In-house pipeline	CNN	Accuracy 90%
[134]	2021	119 subjects (age 0–2 years)	sMRI	In-house pipeline	CNN	MAE 0.98 months
[135]	2021	220 fetuses (gestation age 15.9–38.7 weeks)	sMRI	In-house pipeline	CNN	MAE 0.125 weeks
[136]	2021	167 patients with Rolandic epilepsy (age 9.81 ± 2.55 years), 107 HC (age 9.43 ± 2.57 years)	sMRI	CAT12, SPM12	CNN	MAE 1.05 years for HC 1.21 years for patients
[137]	2022	524 infants (gestation age 23–42 weeks)	sMRI, DTI	Neonatal specific segmentation pipeline	CNN	MAE 0.72 weeks (term-born) 2.21 weeks (preterm)

Abbreviations: sMRI—structural MRI, rs-fMRI—resting-state functional MRI, DTI—Diffusion Tensor Imaging, CNN—Convolutional neural network, GAN—Generative adversarial network, MAE—mean absolute error.

3.4. Predicting Neurodevelopment Outcomes

The relationship between brain structure and cognitive function is complex. Research on brain activity and connectivity builds the network theory to capture the brain trajectories. It remains a challenge in the field of neuroscience to relate basic structural properties of brain to complex cognitive functions [138]. This study reviewed research on correlating brain structure and measurable neurodevelopment outcomes such as fluid intelligence, language function, and motor function (Table 5).

The ABCD dataset provides neuroimaging data including sMRI, rsfMRI, and DTI as well as cognitive assessments such as fluid intelligence and oral reading scores. Large-scale studies based on the ABCD dataset involve thousands of data and a variety of modalities to predict neurodevelopment outcomes [138–142]. CNN models were also employed to predict motor function and cognitive deficits in very preterm infants [143,144].

Table 5. Predicting neurodevelopment outcomes.

Study	Year	Score	Population	Technique	Preprocessing	Method	Results
[143]	2021	Cognitive Deficits	261 very preterm infants (gestation age ≤32 weeks , scan at 39–44 weeks postmenstrual age)	DTI, rs-fMRI	FSL	CNN	Accuracy 88.4%
[145]	2020	Fluid Intelligence	ABCD Study 8333 subjects (age 9–10 years)	sMRI	-	3D CNN	MSE 0.75626
[141]	2021	Fluid Intelligence	ABCD Dataset 7709 subjects (age 9–10 years)	sMRI	FSL, ANFI, FreeSuerfer	CNN	Pearson's correlation coefficient r = 0.18
[138]	2022	Fluid Intelligence	ABCD Dataset 8070 subjects (age 9–11 years) HCP Dataset 1079 subjects (age 22–35 years)	sMRI	FreeSurfer	CNN	MSE 0.919 (ABCD Dataset) 0.834 (HCP dataset)
[140]	2022	Fluid Intelligence	ABCD Dataset 7693 subjects (age 9–11 years)	rs-fMRI	FreeSurfer	CNN	MAE 5.582 ± 0.012
[142]	2022	Fluid Intelligence	ABCD Dataset Training: 3739 subjects, Validation 415 subjects, Testing 4515 subjects (age 9–11 years)	sMRI	FSL, ANFI, FreeSuerfer	CNN	MSE 82.56 for testing
[146]	2021	Language Scores	31 subjects with persistent language concerns (age 4.25 ± 2.38years)	DTI	In-house pipeline	CNN	MAE 0.28
[147]	2021	Language Scores	37 subjects with epilepsy (age 11.8 ± 3.1years)	DTI	FSL	CNN	MAE 7.77

Table 5. *Cont.*

Study	Year	Score	Population	Technique	Preprocessing	Method	Results
[144]	2020	Motor	77 very pre-term infants (gestation age <31 weeks)	DTI	ANTS	CNN	Accuracy 73%
[139]	2021	Oral Reading	ABCD Study 5252 subjects (age 9–10 years)	sMRI, DTI	-	Auto-encoder	MSE 206.5

Abbreviations: sMRI—structural MRI, rs-fMRI—resting-state functional MRI, DTI—Diffusion Tensor Imaging, CNN—Convolutional neural network, MAE—mean absolute error, MSE—mean squared error.

3.5. Optimizing MRI Brain Imaging and Analysis

Assessing imaging quality and optimizing image acquisition are significant for medical imaging analysis. Reconstruction techniques adjust the scanning parameters to maximize the image quality and control the scanning time, which is of great benefit for pediatric imaging in which many subjects cannot stay still for a long time [148]. Furthermore, some scans may be missing or with low quality due to inadequate scanning time or fail completion by the participants. Image generation algorithms synthesize pseudo-images from low-resolution image or latent space, which provide a solution to recapture missing data or rectify scans with low quality [149]. Here, we review the deep learning algorithms for image quality assessment, reconstruction, and synthesis (Table 6).

Image quality assessment tools were constructed with 2D CNN for structural MRI and DTI [150–152]. Study [153] utilized a two-stage transfer learning strategy which showed near-perfect accuracy in evaluating image quality and is capable of real-time large-scale assessment. GANs are widely applied in image generation tasks [149,154–157]. GANs showed great capability in generating synthetic images to implement missing data or improve the signal-to-noise ratio of poor quality images [24,149]. Study [148] proposed CNN models for reconstruction which reduced the scan time by 42% while maintaining image quality and lesion detectability. CNN combined with RNN also showed superior performance in improving the signal-to-noise ratio [24].

Table 6. Optimizing MRI brain imaging and analysis.

Study	Year	Task	Population	Technique	Preprocessing	Method	Results
[158]	2020	Image Enhancement	131 neuro-oncology patients (age 0.4–17.1 years)	ASL	-	Auto-encoder	SNR Gain 62%
[159]	2018	Image Generation	28 infants (scan at birth, 3 months, and 6 months)	DTI	FSL	CNN	MAE 44.4 ± 17.5 (3-month-old from neonates) 40.1 ± 10.6 (6-month-old from 3-month-old)
[154]	2019	Image Generation	16 subjects (age 1.1–21.3 years)	sMRI	-	GAN	MAE 52.4 ± 17.6
[155]	2020	Image Generation	60 subjects (age 2.6–19 years)	sMRI	In-house pipeline	GAN	MAE 61.0 ± 14.1

Table 6. *Cont.*

Study	Year	Task	Population	Technique	Preprocessing	Method	Results
[156]	2022	Image Generation	ABCD Dataset: 1517 subjects (age 9–10 years)	sMRI	-	GAN	PSNR 31.371 ± 1.813
[149]	2022	Image Generation	127 neonates (postmenstrual age = 41.1 ± 1.5 weeks)	sMRI	ANTs	3D GAN	RMAE 5.6 ± 1.1%
[157]	2022	Image Generation	125 subjects (age 1–20 years)	sMRI	FSL	GAN	PSNR 28.5 ± 2.2
[150]	2019	Image Quality Evaluation	ABIDE Dataset: 1112 subjects (age 7–64 years)	sMRI	SPM12	CNN	Accuracy 84%
[153]	2020	Image Quality Evaluation	BCP dataset: 534 images (age 0–6 years)	sMRI	-	CNN	capable of real-time large-scale assessment with near-perfect accuracy.
[151]	2021	Image Quality Evaluation	211 fetuses (gestation age 30.9 ± 5.5 weeks)	sMRI	In-house pipeline	CNN	Accuracy 85 ± 1%
[152]	2022	Image Quality Evaluation	ABCD Dataset: 2494 subjects (age 9–10 years) HBN Dataset: 4226 subjects (age 5–21 years)	DTI	MATRIX, FSL	CNN	Accuracy 96.61% (ABCD Dataset) 97.52% (HBN Dataset)
[160]	2021	Image Reconstruction	20 fetuses (gestation age 23.4–38 weeks)	DTI	SVR pipeline	CNN	RMSE 0.0379 ± 0.0030
[24]	2021	Image Reconstruction	305 subjects (age 0–15 years)	sMRI	In-house pipeline	CNN+RNN	PSNR 27.85+/−2.12
[161]	2022	Image Reconstruction	107 subjects (age 0.2–18 years)	sMRI	-	CNN	image quality improved significantly by qualitative assessment
[148]	2022	Image Reconstruction	47 subjects (age 2.3–14.7 years)	sMRI	-	CNN	Reduce scan time by 42%

Abbreviations: sMRI—structural MRI, ASL—Arterial spin labeling, DTI—Diffusion Tensor Imaging, CNN—Convolutional neural network, GAN—Generative adversarial network, MAE—mean absolute error, PSNR—Peak signal-to-noise ratio.

4. Discussion

4.1. Advancements in Deep Learning Applied to Pediatric MRI

This study reviews pediatric MRI studies for recognition, segmentation, and prediction tasks in neurodevelopment. Throughout the review, CNN is the most commonly utilized model. Variations and advancement based on the basic architecture have been proposed to improve the performance in multi-tasks. Multi-view 2D CNN and 3D CNN have been proposed to deal with the 3D volumes in neuroimaging [57,82,84]. The multi-view 2D CNN processes 3D volumes with slices generated from sagittal, axial, and coronal sections while 3D CNN utilizes 3D kernels in the networks. Multi-branch CNN models also utilize multimodal imaging to study the brain from different perspectives. Structural

connectomes and functional connectomes were combined for age prediction in study [129] and cognitive function prediction in study [139]. Multimodal studies classified children with ASD from healthy controls using combinations of sMRI and rs-fMRI [75,76,81]. sMRI provides structural information, fMRI provides information based on brain activity, and DTI provides information regarding quantitative anisotropy and orientation. Multimodal neuroimaging allows researchers to understand the brain from different perspectives and plays an essential role in investigating the brain functional and structural changes in pediatric neurodevelopment. Variations of U-net dominate in the segmentation tasks. Dilated-Dense U-Net and U-net with attention mechanism achieved great performance in brain structure segmentation [104,120]. Meanwhile, semi-supervised learning and transfer learning initiated studies with a small number of training data [103,122]. GAN shows its superiority in image generation tasks. Variations of GANs have been proposed to synthesize pseudo-images from low-resolution images or latent space [149,155,156]. Overall, the development of computational powers has enabled deep learning models to have more complex structures and greater ability to process 3D volumes for a variety of tasks.

4.2. Challenges and Future Directions

4.2.1. Overfitting Caused by Small Sample Size

Overfitting remains a major concern for deep learning models with deep and complex architectures, especially the models with 3D structures as the number of training parameters grows exponentially with an extra dimension [2]. The sample size should also increase to train models with many parameters to avoid overfitting. Otherwise the model might be overfitted to the training data and fail to predict new data accurately. However, neuroimaging acquisition via MRI is expensive and time-consuming. Many studies are limited to a small number of training data, experiencing the risk of overfitting [162]. In our review, some studies use cross-validation to report results while some others also report results on an independent testing dataset. The testing results are important indicators of the capability to apply the trained model on unseen new data.

Data-sharing projects and platforms provide a vast amount of neuroimaging data, facilitating large-scale studies to train deep and complex models. We share a non-exhaustive list of available public datasets and repositories in Section 2. In common practice, supervised learning, in which the deep learning model is trained with labeled data is the most widely applied learning process [15,163]. Open datasets and repositories prepared data and labels in pairs where labels can be disease diagnosis, clinical outcomes, and semantic segmentation ground truth. Other than labeled data, there are tons of neuroimaging data without labels or with a limited number of labels. Unsupervised learning and semi-supervised learning show great potential in dealing with such data. Unsupervised learning utilizes training data without any labels by separating the data into different categories with automatically learned patterns during training [15,163]. Semi-supervised learning utilizes the unlabeled data to learn the feature patterns and use the labeled data to update model weights, which has yielded superior performance with a limited number of training samples in both classification and segmentation tasks [70,110]. Transfer learning accommodates another possibility for developing deep learning algorithms with a limited number of training data. Transfer learning takes advantage of models pre-trained on large datasets and fine-tunes the system with a small number of data, providing an applicable solution for neuroimaging studies with a small sample size [60,94,97].

4.2.2. Inconsistent Preprocessing Pipelines

Preprocessing is another challenge in pediatric neuroimaging studies. It is necessary to remove the non-brain tissue and noise in many tasks, especially for neuroimaging data of children with significant motion artifacts. However, replication and validation of results are often thus challenged by the variations in data inclusion criteria and preprocessing pipelines. The common preprocessing steps for sMRI include brain extraction, normalization to standard templates, brain tissue segmentation, and brain surface reconstruction [93].

The fMRI preprocessing steps include brain extraction, motion correction, slice time correction, distortion correction, alignment to structural images, and confounds regression [52,90]. The DTI preprocessing steps include distortion correction, Eddy current correction, brain extraction, alignment to structural images, and tensor fitting [60]. The mentioned preprocessing steps may involve multiple preprocessing softwares and adjustments may be applied to different pipelines in different studies. We listed the specified softwares and pipelines in our results. Common preprocessing softwares include SPM [164], AFNI [165], ANTs [166], FSL [167], Dpabi [168], and FreeSurfer [169]. Some studies use in-house preprocessing pipelines or did not specify the preprocessing steps. Preprocessing in single research projects may be time- and effort-consuming while variations of preprocessing pipelines restrict the replication of research results.

Standardization in data preparation and preprocessing is an urgent need for conducting large-scale neuroimaging studies. Fortunately, efforts towards standardization have been contributed by different organizations. Many data-sharing platforms employ the Brain Imaging Data Structure (BIDS) format to adopt a standardized way of organizing neuroimaging and behavioral data [170]. Furthermore, the ABIDE dataset and ADHD200 consortium release both raw and preprocessed data with shared preprocessing pipelines [31,34]. Standardization of preprocessing pipelines will greatly improve the efficacy of neuroimaging studies in the future.

4.2.3. Difficulty in Interpreting Deep Learning Results

Deep learning has been criticized for its "black-box nature" which poses challenges for the interpretability and explainability of trained models, and thus brings concerns to medical decision-making. The deep learning system must provide the rationale behind the decision-making process to make trustworthy predictions [171]. Various approaches have been proposed to interpret deep learning algorithms. One of the common methods is the graph-based visualization approach, which identifies the critical regions for predicting results based on activation maps derived from model weights [172,173]. Study [92] applied such an approach to identify the brain regions where children with ADHD differed from controls. The attention mechanism which focuses selectively on information of interest also plays a vital role in the interpretability of deep learning [174]. Functional connectivity differences between ADHD patients and healthy controls were identified using deep self-attention factorization in the study [90]. There are some other techniques for interpretation such as feature importance and analyzing trends and outliers in predictions. However, studies in this review have not utilized such techniques. Deep model interpretation provides crucial information for understanding brain functions and neurodevelopment, which is of great importance for pediatric neuroimaging studies. Interpretability should be one of the research focuses in future neuroimaging studies.

4.3. Limitations

Although some of the studies did not specify the limitations, there are some common limitations shared across individual studies. Firstly, many studies trained with a limited number of training samples, risking the bias of overfitting. The lack of independent testing results greatly restrains the generalizability of trained models to unseen data. Secondly, architectures of deep neural networks in many studies are trained in a non-exhausted exploration manner that is restricted by computational power. Thirdly, interpretation of the results is lacking in many studies and thus inhibits the interpretability and explainability of trained models. Lastly, for multi-site data which have different scanning protocols, confounding factors might cause risks of bias in the results.

This review systematically organized the most recent research on deep learning applied to pediatric MRI. However, we are unable to include the thousands of results returned by databases GoogleScholar and ScienceDirect, which remains a limitation of the study. Further investigations on unlisted studies may be applied with automatic review tools for paper selection. Keywords selected for the review are not disorder-specific and hence

may neglect some studies optimal for the inclusion criteria but not included in the initial research. Future studies on specific disorders may accommodate the limitations.

5. Conclusions

Deep learning plays an essential role in recent neuroimaging studies. Advancements in applications of deep learning to pediatric neuroimaging have been illustrated in this review. Complex deep learning models such as CNN and GAN have shown superior performance in neuroimaging recognition, prediction, segmentation, and generation tasks. Semi-supervised learning demonstrated great potential in the utilization of weakly labeled or unlabeled data. Challenges such as overfitting, preprocessing variations, and interpretation issues remain in many neuroimaging studies, but data-sharing platforms, standardization of preprocessing protocols, and advanced interpretation approaches have been proposed to tackle such difficulties. Future neuroimaging research on large scales will not only achieve high accuracy but also benefit the understanding of the brain functions and neurodevelopment.

Author Contributions: Writing—original draft preparation, M.H.; writing—review and editing, K.-K.A., H.Z. and C.N. All authors have read and agreed to the published version of the manuscript.

Funding: The research is supported by Institute for Infocomm Research (I2R), Agency for Science, Technology and Research (A*STAR), Singapore, and also by the A*STAR Strategic Programme Funds Project No. C211817001 Brain Body Initiative.

Institutional Review Board Statement: Not applicable.

Informed Consent Statement: Not applicable.

Data Availability Statement: Not applicable.

Conflicts of Interest: The authors declare no conflict of interest.

Abbreviations

The following abbreviations are used in this manuscript:

ABCD	The Adolescent Brain Cognitive Development
ABIDE	Autism Brain Imaging Data Exchange
ADHD	Attention deficit hyperactivity disorder
ASD	Autism spectrum disorder
ASL	Arterial spin labeling
CNN	Convolutional neural network
dHCP	Human Connectomme Project Development
DTI	Diffusion tensor imaging
fMRI	functional MRI
GAN	Generative adversarial network
HBN	Human Brain Network
HC	Healthy control
ICBM	International Consortium for Brain Mapping
IMPAC	Imaging Psychiatry Challenge
MAE	mean absolute error
MLP	Multi-layer perceptron
MRI	Magnetic resonance imaging
MSE	mean squared error
NDAR	National Dtabase for Autism Research
PNC	Philadelphia Neurodevelopmental Cohort
PRISMA	preferred reporting items for systematic reviews and meta-analysis
PSNR	Peak signal-to-noise ratio
rs-fMRI	resting-state fMRI
sMRI	structural MRI

Appendix A. Risk of Bias Analysis

Risk of bias analysis were performed following the Risk Of Bias In Non-randomized Studies of Interventions [48] for (1) risk of bias due to confounding (age, gender, scanning parameters); (2) risk of bias in selection of participants into the study (population, sample size); (3) risk of bias in classification of interventions; (4) risk of bias due to deviations from intended interventions (unexpected results); (5) risk of bias due to missing data; (6) risk of bias arising from measurement of outcomes (assessment parameters, validation protocol, independent testing protocols); (7) risk of bias in selection of reported results.

Each risk of bias is rated with "N"—No, "PN"—Probably No, "PY"—Probably Yes, and "Y"—Yes. Most studies are well-designed and have low risks in most criteria while some studies with small sample sizes have the risk of bias due to confounding, selection of participants, and measurement of outcomes. Studies with at least two "PY"s are rated "Moderate" in the summary. Ratings of individual studies are listed in Table A1.

Table A1. Risk of bias analysis.

Study	Confounding	Selection of Participants	Classification of Interventions	Deviations from Intended Interventions	Missing Data	Measurement of Outcomes	Selection of Reported Results	Summary
[79]	PN	PY	N	N	N	PY	N	Moderate
[80]	N	PY	N	N	N	PY	N	Moderate
[51]	PN	N	N	N	N	PY	N	Low
[81]	PN	PY	N	N	N	PY	N	Moderate
[53]	PN	PN	N	N	N	PY	N	Low
[52]	PN	PY	N	N	N	PY	N	Moderate
[55]	PN	N	N	N	N	PY	N	Low
[82]	PN	N	N	N	N	PY	N	Low
[69]	PN	PY	N	N	N	PY	N	Moderate
[74]	N	PY	N	N	N	PY	N	Moderate
[83]	PN	N	N	N	N	PY	N	Low
[84]	PN	N	N	N	N	PY	N	Low
[85]	N	PY	N	N	N	PY	N	Moderate
[76]	PN	N	N	N	N	PY	N	Low
[54]	PN	N	N	N	N	N	N	Low
[73]	PN	N	N	N	N	PY	N	Low
[86]	N	PN	N	N	N	PY	N	Low
[75]	PN	PN	N	N	N	PY	N	Low
[87]	PN	N	N	PY	N	PY	N	Moderate
[88]	PN	PN	N	N	N	PY	N	Low
[78]	PN	N	N	N	N	N	N	Low
[89]	PN	N	N	N	N	PY	N	Low
[90]	PN	N	N	N	N	PY	N	Low
[91]	PN	PY	N	N	N	N	N	Low
[77]	PN	N	N	N	N	PY	N	Low
[92]	N	PY	N	N	N	PY	N	Moderate
[93]	N	PN	N	N	N	PY	N	Low
[57]	N	PY	N	N	N	PY	N	Moderate
[61]	N	PY	N	N	N	PY	N	Moderate

Table A1. *Cont.*

Study	Confounding	Selection of Participants	Classification of Interventions	Deviations from Intended Interventions	Missing Data	Measurement of Outcomes	Selection of Reported Results	Summary
[62]	PN	N	N	N	N	PY	N	Low
[58]	N	PY	N	N	N	PY	N	Moderate
[70]	N	PN	N	N	N	PY	N	Low
[59]	N	PY	N	N	N	PY	N	Moderate
[60]	N	PY	N	N	N	PY	N	Moderate
[94]	N	PY	N	N	N	PY	N	Moderate
[63]	N	PY	N	N	N	PY	N	Moderate
[64]	N	PN	N	N	N	PY	N	Low
[65]	N	PN	N	N	N	PY	N	Low
[71]	N	PN	N	N	N	PY	N	Low
[95]	PY	PY	N	N	N	PY	N	Moderate
[72]	N	N	N	N	N	PY	N	Low
[66]	N	PN	N	N	N	PY	N	Low
[96]	N	PY	N	N	N	PY	N	Moderate
[67]	N	PY	N	N	N	PY	N	Moderate
[68]	N	PY	N	N	N	PY	N	Moderate
[104]	N	PN	N	N	N	PY	N	Low
[105]	N	PY	N	N	N	PY	N	Moderate
[106]	N	PY	N	N	N	PY	N	Moderate
[99]	N	PY	N	N	N	PY	N	Moderate
[107]	N	PN	N	N	N	PY	N	Low
[98]	N	PY	N	N	N	PY	N	Moderate
[108]	N	PY	N	N	N	PY	N	Moderate
[101]	N	PN	N	N	N	PY	N	Low
[109]	N	PY	N	N	N	PY	N	Moderate
[110]	N	PY	N	N	N	PY	N	Moderate
[111]	N	PY	N	N	N	PY	N	Moderate
[112]	N	PY	N	N	N	PN	N	Low
[113]	N	PY	N	N	N	PY	N	Moderate
[114]	N	PY	N	N	N	PY	N	Moderate
[25]	N	PY	N	N	N	PY	N	Moderate
[102]	N	PN	N	N	N	PY	N	Low
[115]	PN	PN	N	N	N	PY	N	Low
[116]	N	PY	N	N	N	PY	N	Moderate
[117]	N	PY	N	N	N	PN	N	Low
[118]	N	PN	N	N	N	PY	N	Low
[103]	PN	PN	N	N	N	PY	N	Low
[119]	N	PY	N	N	N	PN	N	Low
[120]	N	PY	N	N	N	PY	N	Moderate
[121]	N	PY	N	N	N	PY	N	Moderate
[122]	PN	PN	N	N	N	PY	N	Low
[123]	N	PN	N	N	N	PY	N	Low
[124]	N	PY	N	N	N	PN	N	Low

Table A1. *Cont.*

Study	Confounding	Selection of Participants	Classification of Interventions	Deviations from Intended Interventions	Missing Data	Measurement of Outcomes	Selection of Reported Results	Summary
[125]	N	PN	N	N	N	PY	N	Low
[126]	N	PN	N	N	N	PY	N	Low
[100]	N	PN	N	N	N	PY	N	Low
[97]	N	PN	N	N	N	PY	N	Low
[84]	N	PN	N	N	N	PY	N	Low
[130]	N	N	N	N	N	PY	N	Low
[131]	N	N	N	N	N	PY	N	Low
[132]	PN	N	N	N	N	N	N	Low
[127]	N	PN	N	N	N	PY	N	Low
[129]	N	N	N	N	N	PY	N	Low
[128]	N	PY	N	N	N	PY	N	Moderate
[133]	N	PY	N	N	N	PY	N	Moderate
[134]	N	PN	N	N	N	PY	N	Low
[135]	N	PN	N	N	N	PY	N	Low
[136]	N	PN	N	N	N	PY	N	Low
[137]	N	N	N	N	N	PY	N	Low
[143]	N	PN	N	N	N	PY	N	Low
[145]	PN	N	N	N	N	PY	N	Low
[141]	PN	N	N	N	N	PY	N	Low
[138]	PN	N	N	N	N	PY	N	Low
[140]	PN	N	N	N	N	PY	N	Low
[142]	PN	N	N	N	N	N	N	Low
[146]	N	PY	N	N	N	PY	N	Moderate
[147]	N	PY	N	N	N	PY	N	Moderate
[144]	N	PY	N	N	N	PY	N	Moderate
[139]	PN	N	N	N	N	PY	N	Low
[158]	N	PN	N	N	N	PY	N	Low
[159]	N	PY	N	N	N	PY	N	Moderate
[154]	N	PY	N	N	N	PY	N	Moderate
[155]	N	PY	N	N	N	PY	N	Moderate
[156]	N	N	N	N	N	PY	N	Low
[149]	N	PN	N	N	N	PY	N	Low
[157]	N	PN	N	N	N	PY	N	Low
[150]	PN	N	N	N	N	PY	N	Low
[153]	PN	N	N	N	N	PY	N	Low
[151]	N	PN	N	N	N	PY	N	Low
[152]	PN	N	N	N	N	PY	N	Low
[160]	N	PY	N	N	N	PY	N	Moderate
[24]	N	PN	N	N	N	PY	N	Low
[161]	N	PN	N	N	N	PN	N	Low
[148]	N	PN	N	N	N	PY	N	Low

Abbreviations: N—No, PN—Probably No, PY—Probably Yes.

References

1. Jordan, M.I.; Mitchell, T.M. Machine learning: Trends, perspectives, and prospects. *Science* **2015**, *349*, 255–260. [CrossRef] [PubMed]
2. Celard, P.; Iglesias, E.; Sorribes-Fdez, J.; Romero, R.; Vieira, A.S.; Borrajo, L. A survey on deep learning applied to medical images: From simple artificial neural networks to generative models. *Neural Comput. Appl.* **2022**, *35*, 2291–2323. [CrossRef] [PubMed]
3. LeCun, Y.; Bengio, Y.; Hinton, G. Deep learning. *Nature* **2015**, *521*, 436–444. [CrossRef] [PubMed]
4. Gu, J.; Wang, Z.; Kuen, J.; Ma, L.; Shahroudy, A.; Shuai, B.; Liu, T.; Wang, X.; Wang, G.; Cai, J.; et al. Recent advances in convolutional neural networks. *Pattern Recognit.* **2018**, *77*, 354–377. [CrossRef]
5. Hosny, A.; Parmar, C.; Quackenbush, J.; Schwartz, L.H.; Aerts, H.J.W.L. Artificial intelligence in radiology. *Nat. Reviews. Cancer* **2018**, *18*, 500–510. [CrossRef]
6. Reig, B.; Heacock, L.; Geras, K.J.; Moy, L. Machine learning in breast MRI. *J. Magn. Reson. Imaging JMRI* **2020**, *52*, 998–1018. [CrossRef]
7. Eslami, T.; Almuqhim, F.; Raiker, J.S.; Saeed, F. Machine learning methods for diagnosing autism spectrum disorder and attention-deficit/hyperactivity disorder using functional and structural MRI: A survey. *Front. Neuroinformatics* **2021**, *14*, 575999. [CrossRef]
8. Zhang, Z.; Li, G.; Xu, Y.; Tang, X. Application of artificial intelligence in the MRI classification task of human brain neurological and psychiatric diseases: A scoping review. *Diagnostics* **2021**, *11*, 1402. [CrossRef]
9. Yousaf, T.; Dervenoulas, G.; Politis, M. Advances in MRI methodology. *Int. Rev. Neurobiol.* **2018**, *141*, 31–76. [CrossRef]
10. Pykett, I.L.; Newhouse, J.H.; Buonanno, F.S.; Brady, T.J.; Goldman, M.R.; Kistler, J.P.; Pohost, G.M. Principles of nuclear magnetic resonance imaging. *Radiology* **1982**, *143*, 157–168. [CrossRef]
11. Van Geuns, R.J.M.; Wielopolski, P.A.; de Bruin, H.G.; Rensing, B.J.; van Ooijen, P.M.; Hulshoff, M.; Oudkerk, M.; de Feyter, P.J. Basic principles of magnetic resonance imaging. *Prog. Cardiovasc. Dis.* **1999**, *42*, 149–156. [CrossRef]
12. Huettel, S.A.; Song, A.W.; McCarthy, G. *Functional Magnetic Resonance Imaging*; Sinauer Associates Sunderland: Sunderland, MA, USA, 2004; Volume 1.
13. Mori, S.; Zhang, J. Principles of diffusion tensor imaging and its applications to basic neuroscience research. *Neuron* **2006**, *51*, 527–539. [CrossRef] [PubMed]
14. Colombo, E.; Fick, T.; Esposito, G.; Germans, M.; Regli, L.; van Doormaal, T. Segmentation techniques of brain arteriovenous malformations for 3D visualization: A systematic review. *Radiol. Medica* **2022**, *127*, 1333–1341. [CrossRef] [PubMed]
15. Castiglioni, I.; Rundo, L.; Codari, M.; Di Leo, G.; Salvatore, C.; Interlenghi, M.; Gallivanone, F.; Cozzi, A.; D'Amico, N.C.; Sardanelli, F. AI applications to medical images: From machine learning to deep learning. *Phys. Medica* **2021**, *83*, 9–24. [CrossRef] [PubMed]
16. Khodatars, M.; Shoeibi, A.; Sadeghi, D.; Ghaasemi, N.; Jafari, M.; Moridian, P.; Khadem, A.; Alizadehsani, R.; Zare, A.; Kong, Y.; et al. Deep learning for neuroimaging-based diagnosis and rehabilitation of autism spectrum disorder: A review. *Comput. Biol. Med.* **2021**, *139*, 104949. [CrossRef] [PubMed]
17. Bahathiq, R.A.; Banjar, H.; Bamaga, A.K.; Jarraya, S.K. Machine learning for autism spectrum disorder diagnosis using structural magnetic resonance imaging: Promising but challenging. *Front. Neuroinform.* **2022**, *16*, 949926. [CrossRef] [PubMed]
18. Wang, S.; Di, J.; Wang, D.; Dai, X.; Hua, Y.; Gao, X.; Zheng, A.; Gao, J. State-of-the-Art Review of Artificial Neural Networks to Predict, Characterize and Optimize Pharmaceutical Formulation. *Pharmaceutics* **2022**, *14*, 183. [CrossRef] [PubMed]
19. Krizhevsky, A.; Sutskever, I.; Hinton, G.E. Imagenet classification with deep convolutional neural networks. *Commun. ACM* **2017**, *60*, 84–90. [CrossRef]
20. Szegedy, C.; Liu, W.; Jia, Y.; Sermanet, P.; Reed, S.; Anguelov, D.; Erhan, D.; Vanhoucke, V.; Rabinovich, A. Going deeper with convolutions. In Proceedings of the IEEE Conference on Computer Vision and Pattern Recognition, Boston, MA, USA, 7–12 June 2015; pp. 1–9. [CrossRef]
21. He, K.; Zhang, X.; Ren, S.; Sun, J. Deep residual learning for image recognition. In Proceedings of the IEEE Conference on Computer Vision and Pattern Recognition, Las Vegas, NV, USA, 27–30 June 2016; pp. 770–778. [CrossRef]
22. Huang, G.; Liu, Z.; Van Der Maaten, L.; Weinberger, K.Q. Densely connected convolutional networks. In Proceedings of the IEEE Conference on Computer Vision and Pattern Recognition, Honolulu, HI, USA, 21–26 July 2017; pp. 4700–4708. [CrossRef]
23. Ronneberger, O.; Fischer, P.; Brox, T. U-net: Convolutional networks for biomedical image segmentation. In Proceedings of the International Conference on Medical image Computing and Computer-Assisted Intervention, Munich, Germany, 5–9 October 2015; Springer: Berlin/Heidelberg, Germany, 2015; pp. 234–241. [CrossRef]
24. Li, Z.; Yu, J.; Wang, Y.; Zhou, H.; Yang, H.; Qiao, Z. Deepvolume: Brain structure and spatial connection-aware network for brain mri super-resolution. *IEEE Trans. Cybern.* **2019**, *51*, 3441–3454. [CrossRef]
25. Li, H.; Chen, M.; Wang, J.; Illapani, V.S.P.; Parikh, N.A.; He, L. Automatic Segmentation of Diffuse White Matter Abnormality on T2-weighted Brain MR Images Using Deep Learning in Very Preterm Infants. *Radiol. Artif. Intell.* **2021**, *3*, e200166. [CrossRef]
26. Yuan, J.; Ran, X.; Liu, K.; Yao, C.; Yao, Y.; Wu, H.; Liu, Q. Machine learning applications on neuroimaging for diagnosis and prognosis of epilepsy: A review. *J. Neurosci. Methods* **2021**, *368*, 109441. [CrossRef] [PubMed]
27. Elbattah, M.; Loughnane, C.; Guérin, J.L.; Carette, R.; Cilia, F.; Dequen, G. Variational Autoencoder for Image-Based Augmentation of Eye-Tracking Data. *J. Imaging* **2021**, *7*, 83. [CrossRef] [PubMed]

28. Goodfellow, I.; Pouget-Abadie, J.; Mirza, M.; Xu, B.; Warde-Farley, D.; Ozair, S.; Courville, A.; Bengio, Y. Generative Adversarial Nets. In *Proceedings of the Advances in Neural Information Processing Systems*; Ghahramani, Z., Welling, M., Cortes, C., Lawrence, N., Weinberger, K.Q., Eds.; Curran Associates, Inc.: New York, NY, USA, 2014; Volume 27.
29. Pan, Z.; Yu, W.; Yi, X.; Khan, A.; Yuan, F.; Zheng, Y. Recent progress on generative adversarial networks (GANs): A survey. *IEEE Access* **2019**, *7*, 36322–36333. [CrossRef]
30. Yi, X.; Walia, E.; Babyn, P. Generative adversarial network in medical imaging: A review. *Med. Image Anal.* **2019**, *58*, 101552. [CrossRef]
31. Di Martino, A.; Yan, C.G.; Li, Q.; Denio, E.; Castellanos, F.X.; Alaerts, K.; Anderson, J.S.; Assaf, M.; Bookheimer, S.Y.; Dapretto, M.; et al. The autism brain imaging data exchange: Towards a large-scale evaluation of the intrinsic brain architecture in autism. *Mol. Psychiatry* **2014**, *19*, 659–667. [CrossRef]
32. Di Martino, A.; O'Connor, D.; Chen, B.; Alaerts, K.; Anderson, J.S.; Assaf, M.; Balsters, J.H.; Baxter, L.; Beggiato, A.; Bernaerts, S.; et al. Enhancing studies of the connectome in autism using the autism brain imaging data exchange II. *Sci. Data* **2017**, *4*, 170010. [CrossRef]
33. IMPAC—Imaging-Psychiatry Challenge: Predicting Autism. Available online: https://paris-saclay-cds.github.io/autism_challenge/ (accessed on 15 December 2022).
34. Consortium, T.A. The ADHD-200 consortium: A model to advance the translational potential of neuroimaging in clinical neuroscience. *Front. Syst. Neurosci.* **2012**, *6*, 62. [CrossRef]
35. Sudlow, C.; Gallacher, J.; Allen, N.; Beral, V.; Burton, P.; Danesh, J.; Downey, P.; Elliott, P.; Green, J.; Landray, M.; et al. UK biobank: An open access resource for identifying the causes of a wide range of complex diseases of middle and old age. *PLoS Med.* **2015**, *12*, e1001779. [CrossRef]
36. Payakachat, N.; Tilford, J.M.; Ungar, W.J. National Database for Autism Research (NDAR): Big Data Opportunities for Health Services Research and Health Technology Assessment. *PharmacoEconomics* **2016**, *34*, 127–138. [CrossRef]
37. Poldrack, R.A.; Barch, D.M.; Mitchell, J.P.; Wager, T.D.; Wagner, A.D.; Devlin, J.T.; Cumba, C.; Koyejo, O.; Milham, M.P. Toward open sharing of task-based fMRI data: The OpenfMRI project. *Front. Neuroinform.* **2013**, *7*, 12. [CrossRef]
38. Mazziotta, J.; Toga, A.; Evans, A.; Fox, P.; Lancaster, J.; Zilles, K.; Woods, R.; Paus, T.; Simpson, G.; Pike, B.; et al. A probabilistic atlas and reference system for the human brain: International Consortium for Brain Mapping (ICBM). *Philos. Trans. R. Soc. London. Ser. B Biol. Sci.* **2001**, *356*, 1293–1322. [CrossRef] [PubMed]
39. Yan, C.G.; Craddock, R.C.; Zuo, X.N.; Zang, Y.F.; Milham, M.P. Standardizing the intrinsic brain: Towards robust measurement of inter-individual variation in 1000 functional connectomes. *Neuroimage* **2013**, *80*, 246–262. [CrossRef] [PubMed]
40. Casey, B.J.; Cannonier, T.; Conley, M.I.; Cohen, A.O.; Barch, D.M.; Heitzeg, M.M.; Soules, M.E.; Teslovich, T.; Dellarco, D.V.; Garavan, H. The adolescent brain cognitive development (ABCD) study: Imaging acquisition across 21 sites. *Dev. Cogn. Neurosci.* **2018**, *32*, 43–54. [CrossRef]
41. Thompson, P.M.; Stein, J.L.; Medland, S.E.; Hibar, D.P.; Vasquez, A.A.; Renteria, M.E.; Toro, R.; Jahanshad, N.; Schumann, G.; Franke, B. The ENIGMA Consortium: Large-scale collaborative analyses of neuroimaging and genetic data. *Brain Imaging Behav.* **2014**, *8*, 153–182. [CrossRef]
42. Satterthwaite, T.D.; Elliott, M.A.; Ruparel, K.; Loughead, J.; Prabhakaran, K.; Calkins, M.E.; Hopson, R.; Jackson, C.; Keefe, J.; Riley, M. Neuroimaging of the Philadelphia neurodevelopmental cohort. *Neuroimage* **2014**, *86*, 544–553. [CrossRef]
43. Alexander, L.M.; Escalera, J.; Ai, L.; Andreotti, C.; Febre, K.; Mangone, A.; Vega-Potler, N.; Langer, N.; Alexander, A.; Kovacs, M. An open resource for transdiagnostic research in pediatric mental health and learning disorders. *Sci. Data* **2017**, *4*, 1–26. [CrossRef]
44. Van Essen, D.C.; Ugurbil, K.; Auerbach, E.; Barch, D.; Behrens, T.E.J.; Bucholz, R.; Chang, A.; Chen, L.; Corbetta, M.; Curtiss, S.W. The Human Connectome Project: A data acquisition perspective. *Neuroimage* **2012**, *62*, 2222–2231. [CrossRef]
45. Howell, B.R.; Styner, M.A.; Gao, W.; Yap, P.T.; Wang, L.; Baluyot, K.; Yacoub, E.; Chen, G.; Potts, T.; Salzwedel, A.; et al. The UNC/UMN Baby Connectome Project (BCP): An overview of the study design and protocol development. *NeuroImage* **2019**, *185*, 891–905. [CrossRef]
46. Moher, D.; Liberati, A.; Tetzlaff, J.; Altman, D.G.; Group, P. Preferred reporting items for systematic reviews and meta-analyses: the PRISMA statement. *Ann. Intern. Med.* **2009**, *151*, 264–269. [CrossRef]
47. Tricco, A.C.; Lillie, E.; Zarin, W.; O'Brien, K.K.; Colquhoun, H.; Levac, D.; Moher, D.; Peters, M.D.J.; Horsley, T.; Weeks, L. PRISMA extension for scoping reviews (PRISMA-ScR): Checklist and explanation. *Ann. Intern. Med.* **2018**, *169*, 467–473. [CrossRef] [PubMed]
48. Sterne, J.A.; Hernán, M.A.; Reeves, B.C.; Savović, J.; Berkman, N.D.; Viswanathan, M.; Henry, D.; Altman, D.G.; Ansari, M.T.; Boutron, I.; et al. ROBINS-I: A tool for assessing risk of bias in non-randomised studies of interventions. *BMJ* **2016**, *355*. [CrossRef]
49. Edition, F. Diagnostic and statistical manual of mental disorders. *Am. Psychiatr. Assoc.* **2013**, *21*, 591–643.
50. Morris-Rosendahl, D.J.; Crocq, M.A. Neurodevelopmental disorders-the history and future of a diagnostic concept. *Dialogues Clin. Neurosci.* **2020**, *22*, 65–72. [CrossRef] [PubMed]
51. Dvornek, N.C.; Ventola, P.; Duncan, J.S. Combining phenotypic and resting-state fMRI data for autism classification with recurrent neural networks. In Proceedings of the 2018 IEEE 15th International Symposium on Biomedical Imaging (ISBI 2018), Washington, DC, USA, 4–7 April 2018; IEEE: Piscataway, NJ, USA, 2018; pp. 725–728.

52. Xiao, Z.; Wu, J.; Wang, C.; Jia, N.; Yang, X. Computer-aided diagnosis of school-aged children with ASD using full frequency bands and enhanced SAE: A multi-institution study. *Exp. Ther. Med.* **2019**, *17*, 4055–4063. [CrossRef] [PubMed]
53. Aghdam, M.A.; Sharifi, A.; Pedram, M.M. Diagnosis of autism spectrum disorders in young children based on resting-state functional magnetic resonance imaging data using convolutional neural networks. *J. Digit. Imaging* **2019**, *32*, 899–918. [CrossRef]
54. Li, H.; Parikh, N.A.; He, L. A novel transfer learning approach to enhance deep neural network classification of brain functional connectomes. *Front. Neurosci.* **2018**, *12*, 491. [CrossRef]
55. Leming, M.; Górriz, J.M.; Suckling, J. Ensemble deep learning on large, mixed-site fMRI datasets in autism and other tasks. *Int. J. Neural Syst.* **2020**, *30*, 2050012. [CrossRef] [PubMed]
56. Sibley, M.H.; Swanson, J.M.; Arnold, L.E.; Hechtman, L.T.; Owens, E.B.; Stehli, A.; Abikoff, H.; Hinshaw, S.P.; Molina, B.S.; Mitchell, J.T.; et al. Defining ADHD symptom persistence in adulthood: Optimizing sensitivity and specificity. *J. Child Psychol. Psychiatry* **2017**, *58*, 655–662. [CrossRef]
57. Ceschin, R.; Zahner, A.; Reynolds, W.; Gaesser, J.; Zuccoli, G.; Lo, C.W.; Gopalakrishnan, V.; Panigrahy, A. A computational framework for the detection of subcortical brain dysmaturation in neonatal MRI using 3D Convolutional Neural Networks. *NeuroImage* **2018**, *178*, 183–197. [CrossRef]
58. Zahia, S.; Garcia-Zapirain, B.; Saralegui, I.; Fernandez-Ruanova, B. Dyslexia detection using 3D convolutional neural networks and functional magnetic resonance imaging. *Comput. Methods Programs Biomed.* **2020**, *197*, 105726. [CrossRef]
59. Aminpour, A.; Ebrahimi, M.; Widjaja, E. Deep learning-based lesion segmentation in paediatric epilepsy. In Proceedings of the Medical Imaging 2021: Computer-Aided Diagnosis, Online, 15–19 February 2021; SPIE: Washington, DC, USA, 2021; Volume 11597, pp. 635–641. [CrossRef]
60. Huang, J.; Xu, J.; Kang, L.; Zhang, T. Identifying epilepsy based on deep learning using DKI images. *Front. Hum. Neurosci.* **2020**, *14*, 590815. [CrossRef] [PubMed]
61. Zhang, J.; Li, X.; Li, Y.; Wang, M.; Huang, B.; Yao, S.; Shen, L. Three dimensional convolutional neural network-based classification of conduct disorder with structural MRI. *Brain Imaging Behav.* **2020**, *14*, 2333–2340. [CrossRef] [PubMed]
62. Menon, S.S.; Krishnamurthy, K. Multimodal Ensemble Deep Learning to Predict Disruptive Behavior Disorders in Children. *Front. Neuroinform.* **2021**, *15*, 742807. [CrossRef] [PubMed]
63. Yang, J.; Lei, D.; Qin, K.; Pinaya, W.H.; Suo, X.; Li, W.; Li, L.; Kemp, G.J.; Gong, Q. Using deep learning to classify pediatric posttraumatic stress disorder at the individual level. *BMC Psychiatry* **2021**, *21*, 535. [CrossRef] [PubMed]
64. Jiang, D.; Hu, Z.; Zhao, C.; Zhao, X.; Yang, J.; Zhu, Y.; Liao, J.; Liang, D.; Wang, H. Identification of Children's Tuberous Sclerosis Complex with Multiple-contrast MRI and 3D Convolutional Network. In Proceedings of the 2022 44th Annual International Conference of the IEEE Engineering in Medicine & Biology Society (EMBC), Scotland, UK, 11–15 July 2022; IEEE: Piscataway, NJ, USA, 2022; pp. 2924–2927.
65. Shabanian, M.; Imran, A.A.Z.; Siddiqui, A.; Davis, R.L.; Bissler, J.J. 3D deep neural network to automatically identify TSC structural brain pathology based on MRI. In Proceedings of the Medical Imaging 2022: Image Processing, San Diego, CA, USA, 20–24 February 2022; SPIE: Washington, DC, USA, 2022; Volume 12032, pp. 613–619.
66. Afshar, P.; Mohammadi, A.; Plataniotis, K.N. Brain tumor type classification via capsule networks. In Proceedings of the 2018 25th IEEE international conference on image processing (ICIP), Athens, Greece, 7–10 October 2018; IEEE: Piscataway, NJ, USA, 2018; pp. 3129–3133. [CrossRef]
67. Lee, M.H.; O'Hara, N.; Sonoda, M.; Kuroda, N.; Juhasz, C.; Asano, E.; Dong, M.; Jeong, J.W. Novel deep learning network analysis of electrical stimulation mapping-driven diffusion MRI tractography to improve preoperative evaluation of pediatric epilepsy. *IEEE Trans. Biomed. Eng.* **2020**, *67*, 3151–3162. [CrossRef] [PubMed]
68. Xu, H.; Dong, M.; Lee, M.H.; O'Hara, N.; Asano, E.; Jeong, J.W. Objective detection of eloquent axonal pathways to minimize postoperative deficits in pediatric epilepsy surgery using diffusion tractography and convolutional neural networks. *IEEE Trans. Med. Imaging* **2019**, *38*, 1910–1922. [CrossRef]
69. Yang, M.; Cao, M.; Chen, Y.; Chen, Y.; Fan, G.; Li, C.; Wang, J.; Liu, T. Large-scale brain functional network integration for discrimination of autism using a 3-D deep learning model. *Front. Hum. Neurosci.* **2021**, *15*, 277. [CrossRef]
70. Wu, M.; Shen, X.; Lai, C.; Zheng, W.; Li, Y.; Shangguan, Z.; Yan, C.; Liu, T.; Wu, D. Detecting neonatal acute bilirubin encephalopathy based on T1-weighted MRI images and learning-based approaches. *BMC Med. Imaging* **2021**, *21*, 103. [CrossRef]
71. Sánchez Fernández, I.; Yang, E.; Calvachi, P.; Amengual-Gual, M.; Wu, J.Y.; Krueger, D.; Northrup, H.; Bebin, M.E.; Sahin, M.; Yu, K.H.; et al. Deep learning in rare disease. Detection of tubers in tuberous sclerosis complex. *PLoS ONE* **2020**, *15*, e0232376. [CrossRef]
72. Quon, J.; Bala, W.; Chen, L.; Wright, J.; Kim, L.; Han, M.; Shpanskaya, K.; Lee, E.; Tong, E.; Iv, M.; et al. Deep learning for pediatric posterior fossa tumor detection and classification: A multi-institutional study. *Am. J. Neuroradiol.* **2020**, *41*, 1718–1725. [CrossRef]
73. Li, S.; Tang, Z.; Jin, N.; Yang, Q.; Liu, G.; Liu, T.; Hu, J.; Liu, S.; Wang, P.; Hao, J.; et al. Uncovering Brain Differences in Preschoolers and Young Adolescents with Autism Spectrum Disorder Using Deep Learning. *Int. J. Neural Syst.* **2022**, *32*, 2250044. [CrossRef] [PubMed]
74. Haweel, R.; Shalaby, A.; Mahmoud, A.; Seada, N.; Ghoniemy, S.; Ghazal, M.; Casanova, M.F.; Barnes, G.N.; El-Baz, A. A robust DWT–CNN-based CAD system for early diagnosis of autism using task-based fMRI. *Med. Phys.* **2021**, *48*, 2315–2326. [CrossRef] [PubMed]

75. Mellema, C.J.; Nguyen, K.P.; Treacher, A.; Montillo, A. Reproducible neuroimaging features for diagnosis of autism spectrum disorder with machine learning. *Sci. Rep.* **2022**, *12*, 3057. [CrossRef] [PubMed]
76. Leming, M.J.; Baron-Cohen, S.; Suckling, J. Single-participant structural similarity matrices lead to greater accuracy in classification of participants than function in autism in MRI. *Mol. Autism* **2021**, *12*, 34. [CrossRef] [PubMed]
77. Chen, M.; Li, H.; Fan, H.; Dillman, J.R.; Wang, H.; Altaye, M.; Zhang, B.; Parikh, N.A.; He, L. ConCeptCNN: A novel multi-filter convolutional neural network for the prediction of neurodevelopmental disorders using brain connectome. *Med. Phys.* **2022**, *49*, 3171–3184. [CrossRef]
78. Zhang-James, Y.; Helminen, E.C.; Liu, J.; Franke, B.; Hoogman, M.; Faraone, S.V. Evidence for similar structural brain anomalies in youth and adult attention-deficit/hyperactivity disorder: A machine learning analysis. *Transl. Psychiatry* **2021**, *11*, 82. [CrossRef]
79. Guo, X.; Dominick, K.C.; Minai, A.A.; Li, H.; Erickson, C.A.; Lu, L.J. Diagnosing autism spectrum disorder from brain resting-state functional connectivity patterns using a deep neural network with a novel feature selection method. *Front. Neurosci.* **2017**, *11*, 460. [CrossRef]
80. Li, X.; Dvornek, N.C.; Zhuang, J.; Ventola, P.; Duncan, J.S. Brain biomarker interpretation in ASD using deep learning and fMRI. In Proceedings of the International Conference on Medical Image Computing and Computer-Assisted Intervention, Granada, Spain, 16–20 September 2018; Springer: Berlin/Heidelberg, Germany, 2018; pp. 206–214.
81. Akhavan Aghdam, M.; Sharifi, A.; Pedram, M.M. Combination of rs-fMRI and sMRI data to discriminate autism spectrum disorders in young children using deep belief network. *J. Digit. Imaging* **2018**, *31*, 895–903. [CrossRef]
82. Ke, F.; Choi, S.; Kang, Y.H.; Cheon, K.A.; Lee, S.W. Exploring the structural and strategic bases of autism spectrum disorders with deep learning. *IEEE Access* **2020**, *8*, 153341–153352. [CrossRef]
83. Husna, R.N.S.; Syafeeza, A.; Hamid, N.A.; Wong, Y.; Raihan, R.A. Functional magnetic resonance imaging for autism spectrum disorder detection using deep learning. *J. Teknol.* **2021**, *83*, 45–52. [CrossRef]
84. Kawahara, J.; Brown, C.J.; Miller, S.P.; Booth, B.G.; Chau, V.; Grunau, R.E.; Zwicker, J.G.; Hamarneh, G. BrainNetCNN: Convolutional neural networks for brain networks; towards predicting neurodevelopment. *NeuroImage* **2017**, *146*, 1038–1049. [CrossRef] [PubMed]
85. Gao, K.; Sun, Y.; Niu, S.; Wang, L. Unified framework for early stage status prediction of autism based on infant structural magnetic resonance imaging. *Autism Res.* **2021**, *14*, 2512–2523. [CrossRef] [PubMed]
86. Guo, X.; Wang, J.; Wang, X.; Liu, W.; Yu, H.; Xu, L.; Li, H.; Wu, J.; Dong, M.; Tan, W.; et al. Diagnosing autism spectrum disorder in children using conventional MRI and apparent diffusion coefficient based deep learning algorithms. *Eur. Radiol.* **2022**, *32*, 761–770. [CrossRef]
87. Wang, T.; Kamata, S.I. Classification of structural MRI images in Adhd using 3D fractal dimension complexity map. In Proceedings of the 2019 IEEE International Conference on Image Processing (ICIP), Taipei, Taiwan, 22–25 September 2018; IEEE: Piscataway, NJ, USA, 2019; pp. 215–219.
88. Riaz, A.; Asad, M.; Alonso, E.; Slabaugh, G. DeepFMRI: End-to-end deep learning for functional connectivity and classification of ADHD using fMRI. *J. Neurosci. Methods* **2020**, *335*, 108506. [CrossRef]
89. Tang, Y.; Sun, J.; Wang, C.; Zhong, Y.; Jiang, A.; Liu, G.; Liu, X. ADHD classification using auto-encoding neural network and binary hypothesis testing. *Artif. Intell. Med.* **2022**, *123*, 102209. [CrossRef]
90. Ke, H.; Wang, F.; Ma, H.; He, Z. ADHD identification and its interpretation of functional connectivity using deep self-attention factorization. *Knowl.-Based Syst.* **2022**, *250*, 109082. [CrossRef]
91. Wang, D.; Hong, D.; Wu, Q. Attention Deficit Hyperactivity Disorder Classification Based on Deep Learning. *IEEE/Acm Trans. Comput. Biol. Bioinform.* **2022**, 1. [CrossRef]
92. Uyulan, C.; Erguzel, T.T.; Turk, O.; Farhad, S.; Metin, B.; Tarhan, N. A Class Activation Map-Based Interpretable Transfer Learning Model for Automated Detection of ADHD from fMRI Data. *Clin. EEG Neurosci.* **2022**, *54*, 15500594221122699. [CrossRef]
93. Stanley, E.A.M.; Rajashekar, D.; Mouches, P.; Wilms, M.; Plettl, K.; Forkert, N.D. A fully convolutional neural network for explainable classification of attention deficit hyperactivity disorder. In Proceedings of the Medical Imaging 2022: Computer-Aided Diagnosis, Leicester, UK, 20-21 November 2022; SPIE: Washington, DC, USA, 2022; Volume 12033, pp. 296–301.
94. Attallah, O.; Sharkas, M.A.; Gadelkarim, H. Deep learning techniques for automatic detection of embryonic neurodevelopmental disorders. *Diagnostics* **2020**, *10*, 27. [CrossRef]
95. Artzi, M.; Redmard, E.; Tzemach, O.; Zeltser, J.; Gropper, O.; Roth, J.; Shofty, B.; Kozyrev, D.A.; Constantini, S.; Ben-Sira, L. Classification of pediatric posterior fossa tumors using convolutional neural network and tabular data. *IEEE Access* **2021**, *9*, 91966–91973. [CrossRef]
96. Prince, E.W.; Whelan, R.; Mirsky, D.M.; Stence, N.; Staulcup, S.; Klimo, P.; Anderson, R.C.; Niazi, T.N.; Grant, G.; Souweidane, M.; et al. Robust deep learning classification of adamantinomatous craniopharyngioma from limited preoperative radiographic images. *Sci. Rep.* **2020**, *10*, 1–13. [CrossRef] [PubMed]
97. Nalepa, J.; Adamski, S.; Kotowski, K.; Chelstowska, S.; Machnikowska-Sokolowska, M.; Bozek, O.; Wisz, A.; Jurkiewicz, E. Segmenting pediatric optic pathway gliomas from MRI using deep learning. *Comput. Biol. Med.* **2022**, *142*, 105237. [CrossRef] [PubMed]
98. Asis-Cruz, D.; Krishnamurthy, D.; Jose, C.; Cook, K.M.; Limperopoulos, C. FetalGAN: Automated Segmentation of Fetal Functional Brain MRI Using Deep Generative Adversarial Learning and Multi-Scale 3D U-Net. *Front. Neurosci.* **2022**, *16*, 852. [CrossRef]

99. Sourati, J.; Gholipour, A.; Dy, J.G.; Tomas-Fernandez, X.; Kurugol, S.; Warfield, S.K. Intelligent labeling based on fisher information for medical image segmentation using deep learning. *IEEE Trans. Med. Imaging* **2019**, *38*, 2642–2653. [CrossRef] [PubMed]
100. Peng, J.; Kim, D.D.; Patel, J.B.; Zeng, X.; Huang, J.; Chang, K.; Xun, X.; Zhang, C.; Sollee, J.; Wu, J.; et al. Deep learning-based automatic tumor burden assessment of pediatric high-grade gliomas, medulloblastomas, and other leptomeningeal seeding tumors. *Neuro-oncology* **2022**, *24*, 289–299. [CrossRef] [PubMed]
101. Avisdris, N.; Yehuda, B.; Ben-Zvi, O.; Link-Sourani, D.; Ben-Sira, L.; Miller, E.; Zharkov, E.; Ben Bashat, D.; Joskowicz, L. Automatic linear measurements of the fetal brain on MRI with deep neural networks. *Int. J. Comput. Assist. Radiol. Surg.* **2021**, *16*, 1481–1492. [CrossRef]
102. Zhao, L.; Asis-Cruz, J.; Feng, X.; Wu, Y.; Kapse, K.; Largent, A.; Quistorff, J.; Lopez, C.; Wu, D.; Qing, K.; et al. Automated 3D Fetal Brain Segmentation Using an Optimized Deep Learning Approach. *Am. J. Neuroradiol.* **2022**, *43*, 448–454. [CrossRef]
103. Grigorescu, I.; Vanes, L.; Uus, A.; Batalle, D.; Cordero-Grande, L.; Nosarti, C.; Edwards, A.D.; Hajnal, J.V.; Modat, M.; Deprez, M. Harmonized segmentation of neonatal brain MRI. *Front. Neurosci.* **2021**, *15*, 662005. [CrossRef]
104. Li, G.; Chen, M.H.; Li, G.; Wu, D.; Lian, C.; Sun, Q.; Rushmore, R.J.; Wang, L. Volumetric Analysis of Amygdala and Hippocampal Subfields for Infants with Autism. *J. Autism Dev. Disord.* **2022**, 1–15. [CrossRef]
105. Tor-Diez, C.; Porras, A.R.; Packer, R.J.; Avery, R.A.; Linguraru, M.G. Unsupervised MRI homogenization: Application to pediatric anterior visual pathway segmentation. In Proceedings of the International Workshop on Machine Learning in Medical Imaging 2020, Lima, Peru, 4 October 2020; pp. 180–188. [CrossRef]
106. Sourati, J.; Gholipour, A.; Dy, J.G.; Kurugol, S.; Warfield, S.K. Active deep learning with fisher information for patch-wise semantic segmentation. In Proceedings of the Deep Learning in Medical Image Analysis and Multimodal Learning for Clinical Decision Support: 4th International Workshop, DLMIA 2018, and 8th International Workshop, ML-CDS 2018, Held in Conjunction with MICCAI 2018, Granada, Spain, 20 September 2018; Springer: Berlin/Heidelberg, Germany, 2018; pp. 83–91. [CrossRef]
107. Rutherford, S.; Sturmfels, P.; Angstadt, M.; Hect, J.; Wiens, J.; van den Heuvel, M.I.; Scheinost, D.; Sripada, C.; Thomason, M. Automated brain masking of fetal functional MRI with open data. *Neuroinformatics* **2022**, *20*, 173–185. [CrossRef]
108. Ebner, M.; Wang, G.; Li, W.; Aertsen, M.; Patel, P.A.; Aughwane, R.; Melbourne, A.; Doel, T.; Dymarkowski, S.; De Coppi, P.; et al. An automated framework for localization, segmentation and super-resolution reconstruction of fetal brain MRI. *NeuroImage* **2020**, *206*, 116324. [CrossRef]
109. Bermudez, C.; Blaber, J.; Remedios, S.W.; Reynolds, J.E.; Lebel, C.; McHugo, M.; Heckers, S.; Huo, Y.; Landman, B.A. Generalizing deep whole brain segmentation for pediatric and post-contrast MRI with augmented transfer learning. In Proceedings of the Medical Imaging 2020: Image Processing, Houston, TX, USA, 17–20 February 2020; SPIE: Washington, DC, USA, 2020; Volume 11313, pp. 111–118.
110. Enguehard, J.; O'Halloran, P.; Gholipour, A. Semi-supervised learning with deep embedded clustering for image classification and segmentation. *IEEE Access* **2019**, *7*, 11093–11104. [CrossRef] [PubMed]
111. Khalili, N.; Lessmann, N.; Turk, E.; Claessens, N.; de Heus, R.; Kolk, T.; Viergever, M.A.; Benders, M.J.; Išgum, I. Automatic brain tissue segmentation in fetal MRI using convolutional neural networks. *Magn. Reson. Imaging* **2019**, *64*, 77–89. [CrossRef] [PubMed]
112. Li, H.; Parikh, N.A.; Wang, J.; Merhar, S.; Chen, M.; Parikh, M.; Holland, S.; He, L. Objective and automated detection of diffuse white matter abnormality in preterm infants using deep convolutional neural networks. *Front. Neurosci.* **2019**, *13*, 610. [CrossRef]
113. Grimm, F.; Edl, F.; Kerscher, S.R.; Nieselt, K.; Gugel, I.; Schuhmann, M.U. Semantic segmentation of cerebrospinal fluid and brain volume with a convolutional neural network in pediatric hydrocephalus—transfer learning from existing algorithms. *Acta Neurochir.* **2020**, *162*, 2463–2474. [CrossRef] [PubMed]
114. Yang, R.; Zuo, H.; Han, S.; Zhang, X.; Zhang, Q. Computer-Aided Diagnosis of Children with Cerebral Palsy under Deep Learning Convolutional Neural Network Image Segmentation Model Combined with Three-Dimensional Cranial Magnetic Resonance Imaging. *J. Healthc. Eng.* **2021**, *2021*, 1822776. [CrossRef]
115. Uus, A.U.; Ayub, M.U.; Gartner, A.; Kyriakopoulou, V.; Pietsch, M.; Grigorescu, I.; Christiaens, D.; Hutter, J.; Grande, L.C.; Price, A. Segmentation of Periventricular White Matter in Neonatal Brain MRI: Analysis of Brain Maturation in Term and Preterm Cohorts. In Proceedings of the International Workshop on Preterm, Perinatal and Paediatric Image Analysis, Messina, Italy, 13–15 July 2022; Springer: Berlin/Heidelberg, Germany, 2022; pp. 94–104.
116. Luan, X.; Li, W.; Liu, L.; Shu, Y.; Guo, Y. Rubik-Net: Learning Spatial Information via Rotation-Driven Convolutions for Brain Segmentation. *IEEE J. Biomed. Health Inform.* **2021**, *26*, 289–300. [CrossRef]
117. Quon, J.L.; Chen, L.C.; Kim, L.; Grant, G.A.; Edwards, M.S.; Cheshier, S.H.; Yeom, K.W. Deep learning for automated delineation of pediatric cerebral arteries on pre-operative brain magnetic resonance imaging. *Front. Surg.* **2020**, *7*, 89. [CrossRef]
118. Quon, J.L.; Han, M.; Kim, L.H.; Koran, M.E.; Chen, L.C.; Lee, E.H.; Wright, J.; Ramaswamy, V.; Lober, R.M.; Taylor, M.D.; et al. Artificial intelligence for automatic cerebral ventricle segmentation and volume calculation: A clinical tool for the evaluation of pediatric hydrocephalus. *J. Neurosurg. Pediatr.* **2020**, *27*, 131–138. [CrossRef]
119. Hong, J.; Yun, H.J.; Park, G.; Kim, S.; Laurentys, C.T.; Siqueira, L.C.; Tarui, T.; Rollins, C.K.; Ortinau, C.M.; Grant, P.E.; et al. Fetal cortical plate segmentation using fully convolutional networks with multiple plane aggregation. *Front. Neurosci.* **2020**, *14*, 591683. [CrossRef]

120. Dou, H.; Karimi, D.; Rollins, C.K.; Ortinau, C.M.; Vasung, L.; Velasco-Annis, C.; Ouaalam, A.; Yang, X.; Ni, D.; Gholipour, A. A deep attentive convolutional neural network for automatic cortical plate segmentation in fetal MRI. *IEEE Trans. Med. Imaging* **2020**, *40*, 1123–1133. [CrossRef] [PubMed]
121. Khalili, N.; Turk, E.; Benders, M.; Moeskops, P.; Claessens, N.; de Heus, R.; Franx, A.; Wagenaar, N.; Breur, J.; Viergever, M.; et al. Automatic extraction of the intracranial volume in fetal and neonatal MR scans using convolutional neural networks. *Neuroimage Clin.* **2019**, *24*, 102061. [CrossRef] [PubMed]
122. Wang, Y.; Haghpanah, F.S.; Zhang, X.; Santamaria, K.; da Costa Aguiar Alves, G.K.; Bruno, E.; Aw, N.; Maddocks, A.; Duarte, C.S.; Monk, C.; et al. ID-Seg: An infant deep learning-based segmentation framework to improve limbic structure estimates. *Brain Inform.* **2022**, *9*, 12. [CrossRef]
123. Gruber, N.; Galijasevic, M.; Regodic, M.; Grams, A.E.; Siedentopf, C.; Steiger, R.; Hammerl, M.; Haltmeier, M.; Gizewski, E.R.; Janjic, T. A deep learning pipeline for the automated segmentation of posterior limb of internal capsule in preterm neonates. *Artif. Intell. Med.* **2022**, *132*, 102384. [CrossRef] [PubMed]
124. Park, D.K.; Kim, W.; Thornburg, O.S.; McBrian, D.K.; McKhann, G.M.; Feldstein, N.A.; Maddocks, A.B.; Gonzalez, E.; Shen, M.Y.; Akman, C.; et al. Convolutional neural network-aided tuber segmentation in tuberous sclerosis complex patients correlates with electroencephalogram. *Epilepsia* **2022**, *63*, 1530–1541. [CrossRef] [PubMed]
125. Vafaeikia, P.; Wagner, M.W.; Hawkins, C.; Tabori, U.; Ertl-Wagner, B.B.; Khalvati, F. Improving the segmentation of pediatric low-grade gliomas through multitask learning. In Proceedings of the 2022 44th Annual International Conference of the IEEE Engineering in Medicine & Biology Society (EMBC), Scotland, UK, 11–15 July 2022; IEEE: Piscataway, NJ, USA, 2022; pp. 2119–2122.
126. Madhogarhia, R.; Kazerooni, A.F.; Arif, S.; Ware, J.B.; Familiar, A.M.; Vidal, L.; Bagheri, S.; Anderson, H.; Haldar, D.; Yagoda, S. Automated segmentation of pediatric brain tumors based on multi-parametric MRI and deep learning. In Proceedings of the Medical Imaging 2022: Computer-Aided Diagnosis, Leicester, UK, 10 August 2022; SPIE: Washington, DC, USA, 2022; Volume 12033, pp. 723–731.
127. Hong, J.; Feng, Z.; Wang, S.H.; Peet, A.; Zhang, Y.D.; Sun, Y.; Yang, M. Brain age prediction of children using routine brain MR images via deep learning. *Front. Neurol.* **2020**, *11*, 584682. [CrossRef]
128. Kawaguchi, M.; Kidokoro, H.; Ito, R.; Shiraki, A.; Suzuki, T.; Maki, Y.; Tanaka, M.; Sakaguchi, Y.; Yamamoto, H.; Takahashi, Y.; et al. Age estimates from brain magnetic resonance images of children younger than two years of age using deep learning. *Magn. Reson. Imaging* **2021**, *79*, 38–44. [CrossRef]
129. Niu, X.; Zhang, F.; Kounios, J.; Liang, H. Improved prediction of brain age using multimodal neuroimaging data. *Hum. Brain Mapp.* **2020**, *41*, 1626–1643. [CrossRef]
130. Shabanian, M.; Eckstein, E.C.; Chen, H.; DeVincenzo, J.P. Classification of neurodevelopmental age in normal infants using 3D-CNN based on brain MRI. In Proceedings of the 2019 IEEE International Conference on Bioinformatics and Biomedicine (BIBM), San Diego, CA, USA, 18–21 November 2019; IEEE: Piscataway, NJ, USA, 2019; pp. 2373–2378.
131. Hu, W.; Cai, B.; Zhang, A.; Calhoun, V.D.; Wang, Y.P. Deep collaborative learning with application to the study of multimodal brain development. *IEEE Trans. Biomed. Eng.* **2019**, *66*, 3346–3359. [CrossRef]
132. Qu, T.; Yue, Y.; Zhang, Q.; Wang, C.; Zhang, Z.; Lu, G.; Du, W.; Li, X. Baenet: A brain age estimation network with 3d skipping and outlier constraint loss. In Proceedings of the 2020 IEEE 17th International Symposium on Biomedical Imaging (ISBI), Iowa City, IA, USA, 3–7 April 2020; IEEE: Piscataway, NJ, USA, 2020; pp. 399–403.
133. Shabanian, M.; Wenzel, M.; DeVincenzo, J.P. Infant brain age classification: 2D CNN outperforms 3D CNN in small dataset. In Proceedings of the Medical Imaging 2022: Image Processing, San Diego, CA, USA, 20–24 February 2022; SPIE: Washington, DC, USA, 2022; Volume 12032, pp. 626–633.
134. Wada, A.; Saito, Y.; Fujita, S.; Irie, R.; Akashi, T.; Sano, K.; Kato, S.; Ikenouchi, Y.; Hagiwara, A.; Sato, K.; et al. Automation of a Rule-based Workflow to Estimate Age from Brain MR Imaging of Infants and Children Up to 2 Years Old Using Stacked Deep Learning. *Magn. Reson. Med. Sci.* **2023**, *22*, 57–66. [CrossRef]
135. Hong, J.; Yun, H.J.; Park, G.; Kim, S.; Ou, Y.; Vasung, L.; Rollins, C.K.; Ortinau, C.M.; Takeoka, E.; Akiyama, S.; et al. Optimal method for fetal brain age prediction using multiplanar slices from structural magnetic resonance imaging. *Front. Neurosci.* **2021**, *15*, 1284. [CrossRef]
136. Zhang, Q.; He, Y.; Qu, T.; Yang, F.; Lin, Y.; Hu, Z.; Li, X.; Xu, Q.; Xing, W.; Gumenyuk, V.; et al. Delayed brain development of Rolandic epilepsy profiled by deep learning–based neuroanatomic imaging. *Eur. Radiol.* **2021**, *31*, 9628–9637. [CrossRef]
137. Taoudi-Benchekroun, Y.; Christiaens, D.; Grigorescu, I.; Gale-Grant, O.; Schuh, A.; Pietsch, M.; Chew, A.; Harper, N.; Falconer, S.; Poppe, T.; et al. Predicting age and clinical risk from the neonatal connectome. *NeuroImage* **2022**, *257*, 119319. [CrossRef]
138. Wu, Y.; Besson, P.; Azcona, E.A.; Bandt, S.K.; Parrish, T.B.; Breiter, H.C.; Katsaggelos, A.K. A multicohort geometric deep learning study of age dependent cortical and subcortical morphologic interactions for fluid intelligence prediction. *Sci. Rep.* **2022**, *12*, 17760. [CrossRef]
139. Liu, M.; Zhang, Z.; Dunson, D.B. Graph auto-encoding brain networks with applications to analyzing large-scale brain imaging datasets. *Neuroimage* **2021**, *245*, 118750. [CrossRef]
140. Huang, S.G.; Xia, J.; Xu, L.; Qiu, A. Spatio-temporal directed acyclic graph learning with attention mechanisms on brain functional time series and connectivity. *Med. Image Anal.* **2022**, *77*, 102370. [CrossRef]

141. Saha, S.; Pagnozzi, A.; Bradford, D.; Fripp, J. Predicting fluid intelligence in adolescence from structural MRI with deep learning methods. *Intelligence* **2021**, *88*, 101568. [CrossRef]
142. Li, M.; Jiang, M.; Zhang, G.; Liu, Y.; Zhou, X. Prediction of fluid intelligence from T1-w MRI images: A precise two-step deep learning framework. *PLoS ONE* **2022**, *17*, e0268707. [CrossRef] [PubMed]
143. He, L.; Li, H.; Chen, M.; Wang, J.; Altaye, M.; Dillman, J.R.; Parikh, N.A. Deep multimodal learning from MRI and clinical data for early prediction of neurodevelopmental deficits in very preterm infants. *Front. Neurosci.* **2021**, *15*, 753033. [CrossRef] [PubMed]
144. Saha, S.; Pagnozzi, A.; Bourgeat, P.; George, J.M.; Bradford, D.; Colditz, P.B.; Boyd, R.N.; Rose, S.E.; Fripp, J.; Pannek, K. Predicting motor outcome in preterm infants from very early brain diffusion MRI using a deep learning convolutional neural network (CNN) model. *Neuroimage* **2020**, *215*, 116807. [CrossRef] [PubMed]
145. Han, S.; Zhang, Y.; Ren, Y.; Posner, J.; Yoo, S.; Cha, J. 3D distributed deep learning framework for prediction of human intelligence from brain MRI. In Proceedings of the Medical Imaging 2020: Biomedical Applications in Molecular, Structural, and Functional Imaging, Houston, TX, USA, 18–20 February 2020; SPIE: Washington, DC, USA, 2020; Volume 11317, pp. 484–490.
146. Jeong, J.W.; Banerjee, S.; Lee, M.H.; O'Hara, N.; Behen, M.; Juhasz, C.; Dong, M. Deep reasoning neural network analysis to predict language deficits from psychometry-driven DWI connectome of young children with persistent language concerns. *Hum. Brain Mapp.* **2021**, *42*, 3326–3338. [CrossRef] [PubMed]
147. Jeong, J.W.; Lee, M.H.; O'Hara, N.; Juhász, C.; Asano, E. Prediction of baseline expressive and receptive language function in children with focal epilepsy using diffusion tractography-based deep learning network. *Epilepsy Behav.* **2021**, *117*, 107909. [CrossRef] [PubMed]
148. Kim, E.; Cho, H.H.; Cho, S.; Park, B.; Hong, J.; Shin, K.; Hwang, M.; You, S.; Lee, S. Accelerated Synthetic MRI with Deep Learning–Based Reconstruction for Pediatric Neuroimaging. *Am. J. Neuroradiol.* **2022**, *43*, 1653–1659. [CrossRef] [PubMed]
149. Kaplan, S.; Perrone, A.; Alexopoulos, D.; Kenley, J.K.; Barch, D.M.; Buss, C.; Elison, J.T.; Graham, A.M.; Neil, J.J.; O'Connor, T.G.; et al. Synthesizing pseudo-T2w images to recapture missing data in neonatal neuroimaging with applications in rs-fMRI. *NeuroImage* **2022**, *253*, 119091. [CrossRef]
150. Sujit, S.J.; Coronado, I.; Kamali, A.; Narayana, P.A.; Gabr, R.E. Automated image quality evaluation of structural brain MRI using an ensemble of deep learning networks. *J. Magn. Reson. Imaging* **2019**, *50*, 1260–1267. [CrossRef]
151. Largent, A.; Kapse, K.; Barnett, S.D.; De Asis-Cruz, J.; Whitehead, M.; Murnick, J.; Zhao, L.; Andersen, N.; Quistorff, J.; Lopez, C.; et al. Image quality assessment of fetal brain MRI using multi-instance deep learning methods. *J. Magn. Reson. Imaging* **2021**, *54*, 818–829. [CrossRef]
152. Ettehadi, N.; Kashyap, P.; Zhang, X.; Wang, Y.; Semanek, D.; Desai, K.; Guo, J.; Posner, J.; Laine, A.F. Automated Multiclass Artifact Detection in Diffusion MRI Volumes via 3D Residual Squeeze-and-Excitation Convolutional Neural Networks. *Front. Hum. Neurosci.* **2022**, *16*, 877326. [CrossRef]
153. Liu, S.; Thung, K.H.; Lin, W.; Yap, P.T.; Shen, D. Real-time quality assessment of pediatric MRI via semi-supervised deep nonlocal residual neural networks. *IEEE Trans. Image Process.* **2020**, *29*, 7697–7706. [CrossRef]
154. Wang, C.; Uh, J.; He, X.; Hua, C.h.; Acharya, S. Transfer learning-based synthetic CT generation for MR-only proton therapy planning in children with pelvic sarcomas. In Proceedings of the Medical Imaging 2021: Physics of Medical Imaging, Online, 5–19 February 2021; SPIE: Washington, DC, USA, 2021; Volume 11595, pp. 1112–1118.
155. Maspero, M.; Bentvelzen, L.G.; Savenije, M.H.; Guerreiro, F.; Seravalli, E.; Janssens, G.O.; van den Berg, C.A.; Philippens, M.E. Deep learning-based synthetic CT generation for paediatric brain MR-only photon and proton radiotherapy. *Radiother. Oncol.* **2020**, *153*, 197–204. [CrossRef]
156. Zhang, H.; Li, H.; Dillman, J.R.; Parikh, N.A.; He, L. Multi-Contrast MRI Image Synthesis Using Switchable Cycle-Consistent Generative Adversarial Networks. *Diagnostics* **2022**, *12*, 816. [CrossRef]
157. Wang, C.; Uh, J.; Merchant, T.E.; Hua, C.h.; Acharya, S. Facilitating MR-Guided Adaptive Proton Therapy in Children Using Deep Learning-Based Synthetic CT. *Int. J. Part. Ther.* **2022**, *8*, 11–20. [CrossRef] [PubMed]
158. Hales, P.W.; Pfeuffer, J.; A Clark, C. Combined denoising and suppression of transient artifacts in arterial spin labeling MRI using deep learning. *J. Magn. Reson. Imaging* **2020**, *52*, 1413–1426. [CrossRef]
159. Kim, J.; Hong, Y.; Chen, G.; Lin, W.; Yap, P.T.; Shen, D. Graph-based deep learning for prediction of longitudinal infant diffusion MRI data. In Proceedings of the Computational Diffusion MRI: International MICCAI Workshop, Granada, Spain, 22 September 2018; Springer: Berlin/Heidelberg, Germany, 2019; pp. 133–141. [CrossRef]
160. Karimi, D.; Jaimes, C.; Machado-Rivas, F.; Vasung, L.; Khan, S.; Warfield, S.K.; Gholipour, A. Deep learning-based parameter estimation in fetal diffusion-weighted MRI. *Neuroimage* **2021**, *243*, 118482. [CrossRef] [PubMed]
161. Kim, S.H.; Choi, Y.H.; Lee, J.S.; Lee, S.B.; Cho, Y.J.; Lee, S.H.; Shin, S.M.; Cheon, J.E. Deep learning reconstruction in pediatric brain MRI: Comparison of image quality with conventional T2-weighted MRI. *Neuroradiology* **2022**, *65*, 1–8. [CrossRef] [PubMed]
162. Winterburn, J.L.; Voineskos, A.N.; Devenyi, G.A.; Plitman, E.; de la Fuente-Sandoval, C.; Bhagwat, N.; Graff-Guerrero, A.; Knight, J.; Chakravarty, M.M. Can we accurately classify schizophrenia patients from healthy controls using magnetic resonance imaging and machine learning? A multi-method and multi-dataset study. *Schizophr. Res.* **2019**, *214*, 3–10. [CrossRef]
163. Bishop, C.M.; Nasrabadi, N.M. *Pattern Recognition and Machine Learning*; Springer: Berlin/Heidelberg, Germany, 2006; Volume 4.
164. Tzourio-Mazoyer, N.; Landeau, B.; Papathanassiou, D.; Crivello, F.; Etard, O.; Delcroix, N.; Mazoyer, B.; Joliot, M. Automated anatomical labeling of activations in SPM using a macroscopic anatomical parcellation of the MNI MRI single-subject brain. *Neuroimage* **2002**, *15*, 273–289. [CrossRef]

165. Cox, R.W. AFNI: Software for analysis and visualization of functional magnetic resonance neuroimages. *Comput. Biomed. Res.* **1996**, *29*, 162–173. [CrossRef]
166. Avants, B.B.; Tustison, N.; Song, G. Advanced normalization tools (ANTS). *Insight J.* **2009**, *2*, 1–35.
167. Smith, S.M.; Jenkinson, M.; Woolrich, M.W.; Beckmann, C.F.; Behrens, T.E.J.; Johansen-Berg, H.; Bannister, P.R.; De Luca, M.; Drobnjak, I.; Flitney, D.E. Advances in functional and structural MR image analysis and implementation as FSL. *Neuroimage* **2004**, *23*, S208–S219. [CrossRef]
168. Yan, C.G.; Wang, X.D.; Zuo, X.N.; Zang, Y.F. DPABI: Data processing & analysis for (resting-state) brain imaging. *Neuroinformatics* **2016**, *14*, 339–351. [CrossRef]
169. Fischl, B. FreeSurfer. *Neuroimage* **2012**, *62*, 774–781. [CrossRef] [PubMed]
170. Gorgolewski, K.J.; Auer, T.; Calhoun, V.D.; Craddock, R.C.; Das, S.; Duff, E.P.; Flandin, G.; Ghosh, S.S.; Glatard, T.; Halchenko, Y.O.; et al. The brain imaging data structure, a format for organizing and describing outputs of neuroimaging experiments. *Sci. Data* **2016**, *3*, 160044. [CrossRef] [PubMed]
171. Yang, G.; Ye, Q.; Xia, J. Unbox the black-box for the medical explainable AI via multi-modal and multi-centre data fusion: A mini-review, two showcases and beyond. *Inf. Fusion* **2022**, *77*, 29–52. [CrossRef] [PubMed]
172. Zhou, B.; Khosla, A.; Lapedriza, A.; Oliva, A.; Torralba, A. Learning deep features for discriminative localization. In Proceedings of the IEEE Conference on Computer Vision and Pattern Recognition, Las Vegas, NV, USA, 27–30 June 2016; pp. 2921–2929. [CrossRef]
173. Selvaraju, R.R.; Cogswell, M.; Das, A.; Vedantam, R.; Parikh, D.; Batra, D. Grad-cam: Visual explanations from deep networks via gradient-based localization. In Proceedings of the IEEE International Conference on Computer Vision, Venice, Italy, 22–29 October 2017 ; pp. 618–626. [CrossRef]
174. Guidotti, R.; Monreale, A.; Ruggieri, S.; Turini, F.; Giannotti, F.; Pedreschi, D. A survey of methods for explaining black box models. *ACM Comput. Surv. (CSUR)* **2018**, *51*, 1–42. [CrossRef]

Disclaimer/Publisher's Note: The statements, opinions and data contained in all publications are solely those of the individual author(s) and contributor(s) and not of MDPI and/or the editor(s). MDPI and/or the editor(s) disclaim responsibility for any injury to people or property resulting from any ideas, methods, instructions or products referred to in the content.